

**MONITORING GROWTH
DEVELOPMENT AND YIELD
ESTIMATION OF MAIZE USING
VERY HIGH-RESOLUTION UAV-
IMAGES IN GRONAU, GERMANY**

GHEBREGZIABHER YEMANE TUMLISAN
FEBRUARY, 2017

SUPERVISORS:
Ir. M.C. Bronsveld (Kees)
Dr. M.N. Koeva (Mila)



MONITORING GROWTH DEVELOPMENT AND YIELD ESTIMATION OF MAIZE USING VERY HIGH-RESOLUTION UAV- IMAGES IN GRONAU, GERMANY

GHEBREGZIABHER YEMANE TUMLISAN
Enschede, The Netherlands, FEBRUARY, 2017

Thesis submitted to the Faculty of Geo-Information Science and Earth Observation of the University of Twente in partial fulfilment of the requirements for the degree of Master of Science in Geo-information Science and Earth Observation.
Specialization: Natural Resource Management

SUPERVISORS:
Ir. M.C. Bronsveld (Kees)
Dr. M.N. Koeva (Mila)

THESIS ASSESSMENT BOARD:
Dr. Y.A. Hussin (Chair) NRS Department, ITC
Dr. Francesco C. Nex (External Examiner, ITC-EOS)
Ir. M.C. Bronsveld (First Supervisor)
Dr. M.N. Koeva (Second Supervisor)

DISCLAIMER

This document describes work undertaken as part of a programme of study at the Faculty of Geo-Information Science and Earth Observation of the University of Twente. All views and opinions expressed therein remain the sole responsibility of the author, and do not necessarily represent those of the Faculty.

ABSTRACT

Information on crop height and biomass at different growing stages can provide important indications of growth development and carbon stock in the agroecosystem. Monitoring growth development and studying vegetation phenology are mostly associated with various agricultural phenomena, such as planting, emergence, maturing and harvesting, which play an important role in answering agricultural and environmental management policies. This study is therefore aimed in assessing the application of UAV images in estimating biomass and crop height to provide timely and reliable spatial information to the farmers and decision makers for managing and monitoring growth development of crops during the vegetation period.

Obtaining spatiotemporal information and crop phenological status in agriculture during critical periods of the growing season is very challenging using satellite imagery due to the difficulty of recording with high cloud coverage. So this problem can be solved by using UAV images which can be operated at low altitude (below the clouds). The present study focused on (1) the plant height modelling using Crop Surface Models (CSMs), (2) estimation of biomass and percentage Fractional Vegetation Cover (FVC) using RGB-based vegetation indices, (3) estimation of biomass at harvest using plant height derived from Crop Surface Models (CSMs) and (4) biomass modelling using the combination of plant height and Vegetation indices. UAV flights at different growth stages were carried out with RGB camera over summer maize field in western Germany, Gronau. For accurate crop height estimation, very high-resolution multi-temporal Crop Surface Models (CSMs) were derived. The plant height derived from CSMs were validated by field measured plant heights. The result shows that UAV-based CSMs can accurately estimate plant height at different growing stages, during Tasselling R^2 were found to be 0.68 and during ripening stage 0.85. In order to increase the estimation accuracy of plant height a well and evenly distributed GCP points and accurate UAV data collection is necessary.

RGB-based vegetation indices were also calculated from ortho-mosaicked image to map fractional vegetation cover (FVC) and estimate biomass and plant height. The results indicate the ExG and COM vegetation indices were found best in mapping fractional vegetation cover as compared to the other vegetation indices. Furthermore, fresh and dry biomass was estimated using plant height derived from crop surface models using an exponential regression model which results in good correlation (R^2 ranging from 0.6 - 0.72). Using linear regression model with vegetation indices, ExG was found significant at $p < 0.001$ with a coefficient of determination ($R^2 = 0.51$) during stem elongation stage, followed by ExGR ($R^2 = 0.45$) during inflorescence emergence and heading stage. In addition, multiple linear regression models with combined plant height and vegetation indices were used to estimate biomass. Higher performance was observed when a combined Vegetation indices with plant height were used to estimate fresh and dry biomass than vegetation indices alone with R^2 of ranging from 0.70 - 0.76 at both stem elongation and inflorescence emergence/heading stages. This study may provide an improved guidelines for estimation of fresh and dry biomass at harvest of summer maize crop using very high-resolution multi-temporal UAV data.

Keywords: UAVs, high resolution, crop monitoring, CSMs, FVC, vegetation indices, crop height and biomass

ACKNOWLEDGEMENTS

First of all, I would like to thank the almighty God for his grace, care, protection, and guidance as well as gave me courage, patience, and power in life especially during the 18-month journey of my MSc study to accomplish it successfully.

I would also like to acknowledge with deep gratitude to Joint Japan/World Bank Graduate Scholarship Program (JJ/WBGSP) for providing me a scholarship and an opportunity to pursue my MSc study at ITC, University of Twente, The Netherlands. My special thanks also goes to the Ministry of Agriculture the State of Eritrea and Central Administration zone for supporting and facilitating my leave to Netherlands.

My heartfelt appreciation and sincere gratitude also goes to my supervisors, Ir. M.C. Bronsveld and Dr. M.N. Koeva for your constructive criticism, ideas, motivation, patience and always being readily available to advise and support during my entire MSc thesis period. Your timely suggestions and kindness give me courage and motivation throughout the course of the whole thesis. Working under your supervision was really wonderful and I have learned a lot from you on how to think critically and from your perseverance during field work of UAV image collection as well. Also, I would like to express my appreciation to all ITC staffs who performed/participated in UAV flight periods especially M. Gerke (Markus), W.S. Siderius (Watse), C.M. Gevaert (Caroline) and E.C. Stöcker MSc (Claudia). Further appreciation goes to C. Lievens (Caroline) head Geo-Science Laboratory for her advice and technical support during my laboratory analysis. I also wish to thank the chair, Dr. Y.A. Hussin (Yousif) for his constructive comments and suggestions during the proposal and midterm presentations, not forgetting a great support from Drs. E.H. Kloosterman (Henk), I will never forget his advice and encouragement during my studies and finally, I would like to thank Dr.ir. T.A. Groen (Thomas) for giving me statistical ideas during my studies when needed.

My thanks also goes to the farmer, owner of the maize field, who gave us permission for UAV flights and field work measurements on his farm to perform this study during the whole growing season. The study could not have been accomplished without his cooperation.

I am very grateful to thank ITC NRM department staffs with Drs. R.G. Nijmeijer (Raymond) course coordinator and student affairs who tirelessly helped and guided us from the very beginning of our arrival at ITC till the end to comfortably accomplish our studies.

I would like to express my deep gratitude to my fellow students NRM and GEM class of 2015-2017, Specially Semhar, Fetene, John Reuben, Tesfaye, Weicheng, Paulina and our student representative Lucas De Oto, we had a wonderful and unforgettable 18-month journey together with moral support, friendship, inspiration and companionship throughout the entire study.

Last but not least, I would like to express my heartfelt love and appreciation to my family members (my Father, Mother, sister and brother) and my wife for their moral encouragement and support during my studies. Finally, I would like to thank my friends who encouraged me to accomplish my career.

TABLE OF CONTENTS

LIST OF FIGURES	iv
LIST OF TABLES.....	vi
LIST OF ABBREVIATIONS	vii
1. Introduction.....	1
1.1. Background and justification.....	1
1.2. Literature Review.....	2
1.3. Problem statement	4
1.4. Research objectives	4
1.5. Research Questions.....	5
1.6. Research Hypothesis.....	5
2. Study Area and Datasets.....	6
2.1. Study area.....	6
2.2. Data and Materials.....	7
2.2.1. Materials and Software used.....	7
2.2.2. Unmanned Aerial Vehicle (UAV).....	7
2.2.3. Flight planning and UAV Data Acquisition	8
2.2.4. Maize Development stages	9
3. Methodology.....	11
3.1. UAV Data Processing.....	11
3.1.1. Image Pre-processing.....	12
3.1.2. Generation of Mosaicked Orthophoto and Crop Surface Models (CSMs)	14
3.1.3. Spectral Vegetation Indices (VIs) Extraction.....	15
3.1.4. Computation of Fractional Vegetation Cover (FVC)	15
3.2. Field Data Collection for Height and Biomass	17
3.3. Statistical analysis.....	17
4. Results and Discussion	19
4.1. Vegetation Indices and Fractional Vegetation Cover (FVC).....	19
4.2. Crop Surface Models (CSMs) for Plant Height Estimation	21
4.3. Empirical models for biomass assessment at harvest	25
4.3.1. Vegetation Indices modeling for yield assessment	25
4.3.2. Field Measured Plant Height and Biomass Relationship	29
4.3.3. Plant Height (PH _{CSM}) modeling for biomass estimation.....	30
4.3.4. Biomass modeling from the combined VIs and Plant Height (PH _{CSM})	32
4.4. Maize Yield at Harvest	34
5. Conclusion and Recommendation.....	36
5.1. Conclusions	36
5.2. Recommendations.....	38
LIST OF REFERENCES.....	39
APPENDICES.....	44

LIST OF FIGURES

Figure 1: The location map of the study area in Gronau, Germany: (a) Germany Administrative boundaries (provinces); (b) boundary of North Rhine-Westphalia province with Base map world Imagery; and (c) UAV Ortho-mosaicked RGB image, acquired on 08-July-2016.....6

Figure 2: (a) UAV Phantom 4 mounted with RGB bands along with its controlling mechanism (Source: www.dji.com) and (b) Artificial marks for Ground Control Point (GCP) measurement.8

Figure 3: Example of raw images taken by the UAV on June 07, June 16 and July 08, 2016.....9

Figure 4: Maize growth development stages along with the UAV image acquisition dates and field Plant height and Biomass measurements.....10

Figure 5: Flow chart showing image pre-processing in Pix4D software for the generation of Digital Surface Model and Mosaicked Orthophoto, and further analysis in ArcGIS, ENVI classic and Microsoft excel.11

Figure 6: Image processing in pix4D for generation of DSM and Ortho-mosaic; (a) camera positions along with flight route; (b) steps of processing options; and (c) GCP manager for importing GCPs to geo-reference the image.12

Figure 7: Screen shot of camera positions and geo-located images; (a) Automatic tie points and point cloud; (b) densified point cloud and mesh.....13

Figure 8: Final output of Pix4D; (a) Ortho-mosaicked image; and (b) Digital Surface Model (DSM).....14

Figure 9: Multi-temporal crop surface models (CSMs) at different growing stages (Nora Tilly, 2015).....14

Figure 10: (a) True color image; (b) ExG Image; (c) ExG histogram with the different thresholds ($r1 - 15$); and (d&e) classified images with different thresholds (green vegetative and yellow non-vegetative) right after applying VIs and threshold to differentiate vegetative and non-vegetative pixels.....16

Figure 11: Single band classified image (FVC map) obtained from the ExG vegetation index upper image and Mosaicked orthophoto with RGB bands lower image (16-Jun-2016).20

Figure 12: Field measured Plant Height in relation to plant Height derived from CSMs (a) at 18-Aug-2016 and (b) at 20-Sep-2016.21

Figure 13: Plant heights from Crop Surface Model of field two (a) during flight_4 (08-Jul-2016); (b) during flight_5 (27-Jul-2016).22

Figure 14: An example of crop growth development of low, medium and high growing plots through time.22

Figure 15: Crop Surface Models (CSMs) at different dates; the gray surface is the reference ground model (obtained from 7-Jun-2016) and the colored surfaces are the CSMs of different (dates from 16-Jun to 20-Sep-2016).23

Figure 16: Cross-validation relationships of fresh/dry biomass, height and Vegetation indices of different dates; (08-Jul-16) ExG *versus* biomass and height (**a-c**); (27-Jul-16) CIVE and ExGR *versus* biomass and height (**d-i**); and (09-Aug-16) ExG *versus* biomass (**j-k**)..... 25

Figure 17: Graphs showing the relationship between field-measured plant height and biomass at physiological maturity (right before harvesting) on sept. 15-23, 2016..... 29

Figure 18: Cross-validation relationships between fresh/dry Biomass and plant height derived from Crop Surface Models (CSMs); $p < 0.001$ for all R^2 except for 09-Aug-2016, $p < 0.05$ 31

Figure 19: Cross-validation scatter plots for observed fresh and dry biomass versus predicted biomass from the combination of CSM plant height and vegetation indices of dates; 08-Jul-16 (**a&b**); 27-Jul-16 (**c&d**); and 09-Aug-16 (**e&f**)..... 33

Figure 20: Pixel based yield map resulted from modeling of Excess Green (**ExG**) vegetation index and plant height derived from Crop Surface Model (**PH_{CSM}**) of UAV image acquired during Stem elongation of maize..... 35

LIST OF TABLES

Table 1: List of Fieldwork materials and software.....	7
Table 2: UAV-image data acquisition periods and Number of images acquired.....	8
Table 3: The vegetation indices computed based on visible spectral bands.....	15
Table 4: Percentage vegetation fraction, the selected threshold and classification accuracy of each vegetation indices obtained from the Ortho-mosaic at 07-June, 16-June, 08-July, and 27-July.....	19
Table 5: The regression relationships between fresh and dry biomass, Plant Height derived from CSMs Modelled from different vegetation indices and plant height, where R^2 = coefficient of determination; RMSE = root mean square error and nRMSE = normalized root mean square error.	27
Table 6: Coefficient of determination (R^2) for crop heights (PH_{CSM} and PH_{ref} , linear regression) and Plant Height with Fresh and dry biomass (exponential regression) for all plots; at $p < 0.001$. (PH_{CSM} = Crop Surface Model Plant Height; and PH_{ref} = Field measured Plant Height).	29
Table 7: Descriptive statistics field measured plant height and CSMs plant height and aboveground fresh and dry biomass of maize of plots (N=40 for PH_{ref} and biomass; and N=27 for PH_{CSMs}) collected between 15-Sept to 23-Sept-2016, (CV = Coefficient of Variation; SD = Standard Deviation).....	30
Table 8: Multiple linear regression relationships between fresh/dry biomass as an independent variable and VIs together with CSM plant height as independent variables with their respective R^2 , RMSE, and nRMSE values.....	32
Table 9: Descriptive statistics of the actual and predicted biomass (fresh and dry) of maize at harvest (Kg/m^2).....	35

LIST OF ABBREVIATIONS

AGB :	Above Ground Biomass
AOI :	Area Of Interest
CIVE :	Color Index of Vegetation
COM :	Combination
CP :	Check Point
CSM :	Crop Surface Model
DGPS	Differential Global Positioning System
DSM :	Digital Surface Model
DTM :	Digital Terrain Model
ExG :	Excess Green
ExGR :	Excess Green minus Red
FVC :	Fractional Vegetation Cover
GCP :	Ground Control Point
GNSS :	Global Navigation Satellite System
GPS :	Global Positioning System
LAI	Leaf Area Index
LiDAR	Light Detection And Ranging
NGRDI :	Normalized Green-Red Difference Index
nRMSE :	Normalized Root Mean Square Error
PH _{CSM} :	Crop Surface Model Plant Height
PH _{ref} :	Ground reference Plant Height
RMSE :	Root Mean Square Error
UAV :	Unmanned Aerial Vehicle
VEG :	Vegetetiven
VI _s :	Vegetation Indices

1. INTRODUCTION

1.1. Background and justification

World's population is continuously increasing and it is obvious that the need for food, shelter and other basic needs from the limited land resources are also increasing. Therefore, the study of agricultural crop production is very crucial to improve land productivity, generate income and provide food security to people. Important information to improve agricultural production sustainably can be obtained from crop type maps and area extent. This area estimation and crop identification can be obtained from aerial photographs and multispectral satellite imagery using remote sensing acquisition techniques (Yang et al., 2010). For sustainable agricultural production, the study of crop phenology via biomass estimation helps to understand the state of the ecosystem and environmental factors that affect the crop growth (Ajaere, 2012).

Remote sensing data is very important in the field of agriculture especially in the study of climate, soil, land classification and crop inventory (Steven & Clark, 2013). In order to have good yield predictions in agricultural crop production, it is essential to know the type of crops and their areas grown in a region which provides basic information for crop management and agricultural planning. Agricultural crop type mapping and identification throughout the vegetation period provides a vital information to agricultural institutions and stakeholders for their efficient management and monitoring (Inglada et al., 2015).

During the growing season, the height of crops provides an important information on crop health and their response to the environmental effects, such as precipitation and chemical/fertilizer treatment. Height estimates of the tops of crop and the ground, the difference of which is the height of the crop, is the main requirement for crop measurement (Anthony et al., 2014). Manual crop height measurement is expensive, time-consuming and causes damage to the crops because of the unobstructed movement in the field. However, height measurement from the air is also challenging, since the layers of plant leaves obscure the ground. Anthony et al., (2014) also described some techniques that can solve this problem are, (1) Using the increased sensing power radar or LiDAR and (2) Micro-UAV (Unmanned Aerial Vehicle) equipped less powerful sensor operating at low altitude (close to the crops) to capture the small gaps between the crops and sense directly to the ground and lower levels of the vegetation and (3) Using very high resolution digital aerial images taken from airplane.

Ajaere, (2012) noted that biomass/yield estimation and monitoring of agricultural crops (maize crop in this case) are essential because agricultural crops play an important role in the environment. The temporal and spatial resolution of remote sensing datasets help to improve the applicability of remote sensing methods, that is, getting the biophysical parameters of crops during the growing season with very high geometric resolution become easier (Dahms et al., 2016). The accurate estimation of biophysical variables such as Leaf Area Index (LAI), height, and biomass can be used to describe the architecture of plants, monitor changes, and predict growth and yield during the growing season that improves planning and management of crop production (Gao et al., 2013). Economical and quantitative estimation of crop biomass during the growing season is an important ecological indicator of plant growth for crop production management and planning (Li et al., 2015). Crop type mapping and study of vegetation phenology are mostly associated with various agricultural phenomena, such as planting, emergence, maturing and harvest, play an important role in

answering economic and environmental management policies (Reed et al., 1994; Vaudour et al., 2015; Rembold et al., 2013).

Thus, the use very high-resolution multi-temporal UAV images for monitoring crop development during the whole growing seasons is crucial in monitoring, planning and decision making of crop production. Substantial information on agriculture like determining crops, biomass estimation and crop health during their growing season can help farmers and decision makers to monitor and manage the crops in order to get a reasonable yield.

1.2. Literature Review

Although coarse spatial resolution data can provide relevant information in monitoring and managing crop production but has also some disadvantages, so the need for high spatial resolution data is vital. Rembold et al., (2013) insisted in their study that, images obtained from low-resolution satellite imagery (with spatial resolution between 250m to 1km) have been widely used for crop monitoring for over three decades, vegetation performance detected from these low-resolution images have some limitations created by mixed nature of low-resolution pixels. In monitoring agricultural crops the development of high spatial and temporal resolution satellite sensors are opening new opportunities for researchers. New satellites like Sentinel-1 & -2, SPOT5, QuickBird, GeoEye and Worldview-1 & -2 can provide very high spatial, temporal, spectral and radiometric resolution images which can be used to extract information in crop monitoring and management (Richter et al., 2016).

Since the early days of remote sensing crop development and growth have been monitored by the use of satellite images (Rembold et al., 2013), and crop monitoring is essential in precision agriculture. Zhang & Kovacs, (2012) defined Precision Agriculture (PA) as “a farming management strategy that uses information technology to identify variations in the field and deal with them with alternative scenarios to help decisions associated with crop production”. In precision agriculture, the use of unmanned aerial vehicles has been increasing as an alternative to very high cost and not readily available satellite or airborne imageries (Jannoura et al., 2015). The use of very low cost and very high-resolution aerial imagery obtained from radio controlled model aircraft was evaluated by Hunt et al., (2005) to estimate the nutrient status of maize and crop biomass of maize, alfalfa, and soybeans.

Based on the cultural operation of farmers in different regions of the world the use of very high spatial resolution images is essential to map bare soil surface and early season crop identification (Vaudour et al., 2015). Monitoring crops throughout the growing season is the main requirement in precision agriculture, i.e. the application of geospatial information and sensors to identify variation in agricultural fields. It is one of the most imperative practices in the development of sustainable agricultural production (Zhang & Kovacs, 2012). The stages of precision agriculture are data collection & analysis, field variability mapping, and crop management practice. Thus, these processes can be easily done using remotely sensed imagery, particularly, very high-resolution satellite imagery or UAV images which are now readily available at low cost to study soil condition and crops during the growing season.

In monitoring crop growth development determining agricultural plant parameters such as plant height, biomass, plant nitrogen content, Leaf Area Index (LAI) etc. are very essential. Hoffmeister et al., (2010) used Crop Surface Models (CSMs), Crop Volume Model (CVM) and multi-temporal roughness of different crops to estimate the crop parameters. The height of the crops is the difference between the UAV-sourced Digital Surface Model (DSM), equivalent to CSMs in this case, at full canopy and the topography of the field

(DTM) (Waypoint Drone Insight and Inspiration, 2015). Comparison of CSMs at different growing stages helps to determine the crop growth development and estimation of plant height (Juliane Bendig et al., 2013). Hoffmeister et al., (2010) has already introduced the concept of generation of Crop Surface Models using Terrestrial Laser Scanning (TLS). In addition to this Bendig et al., (2013) demonstrated the estimation of biomass of barley by using Crop Surface Models (CSMs) derived from UAV images.

Remote sensing products such as vegetation Indices, derived from visible spectral bands in this case, and plant height derived from CSMs provide measures of amount and condition of green vegetation on the farm land and also gives information on biomass estimation for agricultural management strategies (Geipel et al., 2014; Duncan et al., 2015). Jannoura et al., (2015) also studied the relationships of visible band vegetation indices (like NGRDI) with above ground biomass and Leaf Area Index (LAI) of different crops like oats and peas from UAV data. Similarly, Leaf Area Index and crop biomass estimation of maize and soybean crops were assessed using RapidEye vegetation indices (Kross et al., 2015). A review of remote sensing methods of assessing crop biomass using vegetation indices is presented by Prabhakara et al., (2015); Jannoura et al., (2015); Jin et al., (2015); Kross et al., (2015) and Sharma et al., (2016).

Reflectance properties of crops like vegetation indices are also very essential in studying the performance of crops under different stress which directly affects the yield/biomass. For example, the crop growth development of maize under low nitrogen stress was studied by Zaman-Allah et al., (2015) and Vergara-díaz et al., (2016) using NDVI as well as RGB-based vegetation indices derived from UAV spectral imaging, according to their results these vegetation indices have good performance in assessing crop growth development and spatial field variations of the crops under low N-stress. A medium-resolution data (TM, ETM+) can be used for monitoring spatial and temporal dynamics of vegetation changes, extraction of vegetation cover and growth status of the crops using NDVI vegetation index, which has a comprehensive reflection for vegetation type and cover form (Cui et al., 2011). Estimating Fractional Vegetation Cover (FVC) from vegetation indices also helps in monitoring and modeling vegetation productivity and yield estimations and remote sensing are an advanced science which helps in estimating vegetation cover (Liu et al., 2012).

Unmanned aerial vehicle (UAV) platforms flying at low altitude are used to acquire high temporal and spatial resolution aerial data that enables users to take informed and targeted action. UAVs make use of small compact camera, navigation systems, reliable GPS units and radio receivers to acquire vertical well defined high-resolution images (Tellidis & Levin, 2014). Aerial imagery obtained from Unmanned Aerial Vehicles (UAVs) allows cheap, flexible acquisition and provides high spatial resolution data with high temporal frequencies (Centre for Earth Systems Engineering Research (CESER), n.d.). The CESER also described the monitoring of Vegetation phenology, land use land cover change, hydrological phenomena, and infrastructure systems can easily be studied using this UAVs imagery.

UAVs can fly at low altitudes and are also capable of observing small individual plants and patches, acquire images even on cloudy days and can also be used in high-risk situations and inaccessible areas (J. Torres-Sánchez et al., 2014). UAVs are also a potential for 3D image generation, capability of decentralized data acquisition (substantial advantage to communities, end users, organization, and government agencies) and can be used for monitoring of illegal activities like illegal timber extraction (Paneque-Gálvez et al., 2014). There are also some limitations for UAV application some of which are small area coverage; they can be affected by wind speed during image acquisition, lack of precise rule framework and tedious requests for flight permissions limits their application (Nex & Remondino, 2014). Paneque- Gálvez et al., (2014) also listed some limitations of UAVs like Poor geometric and radiometric performance, short flight endurance, small payload and the possibility of collisions.

1.3. Problem statement

The decrease in biomass and yield of crops in agricultural fields focussed an attention on the need for high-quality monitoring systems during the growing seasons. Field based crop surveying and production estimates have a potential to give accurate results but it is costly and time-consuming which can lead to a situation of under-sampling which compromise the accuracy measurements and estimates. To overcome this problem the use of satellite data have been increasingly used for achievable goals for growth development health monitoring of crops (Barret et al., 2000), crop production estimation (Lewis et al., 1998) and crop mapping (Jain et al., 2013). The most important step in assessing the application of remote sensing for agricultural monitoring and management is mapping vegetation crop in the field during the growing season, however the use of aerial platforms such as planes and satellites are not suitable for these applications due to their low spatial and temporal resolutions (J. Torres-Sánchez et al., 2014).

The study of non-destructive methods of measuring plant height and changes in plant height over time at high spatial and temporal resolution is essential in crop monitoring studies. In recent years new aerial platform, using remotely controlled UAVs, for image acquisition are progressively increasing and problems related to spatial and temporal resolutions can be solved (Jorge Torres-Sánchez et al., 2013). High-resolution imagery produced by UAVs can be a suitable acquisition technique for monitoring crop development during the growing season, and it is very cheap compared to satellite images, LiDAR, and very high-resolution images from a conventional airplane. It also provides important supplementary information for the assessment of crop health and development. Assessment of early detection of crop infestation as well as crop health is critical in guaranteeing good agricultural productivity and stress like excessive moisture, insects, fungal and weed infestations, and must be detected early enough to provide an opportunity for the farmer to mitigate (Natural Resources Canada, 2015).

Despite the promise of satellite and UAV data of high spatiotemporal resolution for monitoring and crop yield estimates, until present, only a few studies have been made on this issue especially in our study site. Obtaining spatiotemporal information and crop phenological status in agriculture during critical period of the growing season is very challenging using satellite imagery due to the possibility of high cloud coverage. Therefore, this problem can be easily solved by using Very high-resolution UAV (Unmanned Aerial Vehicle) images which can be operated at low altitude (below the clouds). This study is going to assess the application of UAVs in providing timely and reliable (spatial) information to the farmers and decision makers for monitoring growth development of crops during the vegetation period. Due to very high resolution, low cost, high maneuverability, and easy maintenance UAVs are nowadays becoming powerful sensors in scientific researches (Cai et al., 2014). This study aims to provide accurate plant height and maize yield estimates at farm level during the crop growing season.

1.4. Research objectives

The main objective of this research is to provide an accurate plant height and maize yield estimations for monitoring growth development during the growing season in Gronau, Germany, using very high-resolution multi-temporal UAV- images.

To achieve this general objective, the following specific objectives were defined.

1. To assess the best VIs for yield estimation and map Fractional Vegetation Cover (FVC) at different growing stages.
2. Assess the relationship between different RGB-based vegetation indices and yield/biomass and plant height derived from CSMs at different growing stages.
3. To assess and validate the relationship between plant heights derived from CSMs and infield plant height measurement.
4. To assess the relationship between the heights of the crops derived from CSMs and Yield (in terms of biomass).
5. To assess and investigate the best single time to record the maize using UAVs for accurate yield estimation.

1.5. Research Questions

1. Which vegetation index/indices is/are best for fractional vegetation cover mapping in relation to time/growth stage of the crops?
2. What is the accuracy of crop surface models to calculate plant height?
3. Which Vegetation Index is best to estimate maize yield and how is it related to the crop height and yield during the growing season?
4. What are the relationships of biomass versus crop height derived from CSMs and biomass versus Vegetation indices?
5. Which growth stage or best time to record the crop using UAVs for accurate yield estimation?

1.6. Research Hypothesis

1. **H₀:** There is a significant relationship (correlation) between Fractional Vegetation Cover (FVC) obtained from classified RGB image and vegetation indices calculated from visible spectral bands of UAV images at different growing stages.
H₁: There is no significant relationship between FVC and vegetation indices.
2. **H₀:** Crop Surface Models can calculate crop height accurately (>80%) using very high-resolution UAV images.
H₁: Crop Surface Models can calculate crop height with an accuracy (<80%).
3. **H₀:** The vegetation indices calculated from RGB-based UAV images acquired at different dates have a significant relationship with plant height and biomass at the end growing season.
H₁: There is no significant relationship between vegetation indices and plant height or end Fresh/dry biomass.
4. **H₀:** The Crop Surface Models calculated from RGB-based UAV images acquired at different dates have a significant relationship with biomass at the end growing season.
H₁: There is no significant relationship between Crop Surface Models and end Fresh/dry biomass at the end growing season.

2. STUDY AREA AND DATASETS

2.1. Study area

The study was carried out on a maize field (an individual farmer's field) which is located in the North Rhine-Westphalia province of Germany (52° 10'N, 6° 55'E), About 8 km to the south of Enschede, 8 km to the west of Gronau and 13 km Northwest of Ahaus city (fig.1). And it contains two maize fields of around 8 hectares each. During summer months the long term average temperature across this area is 17°C and during winter months 1°C and annual precipitation are between 700 and 800 mm (North-Rhine-Westphalia, 2016).

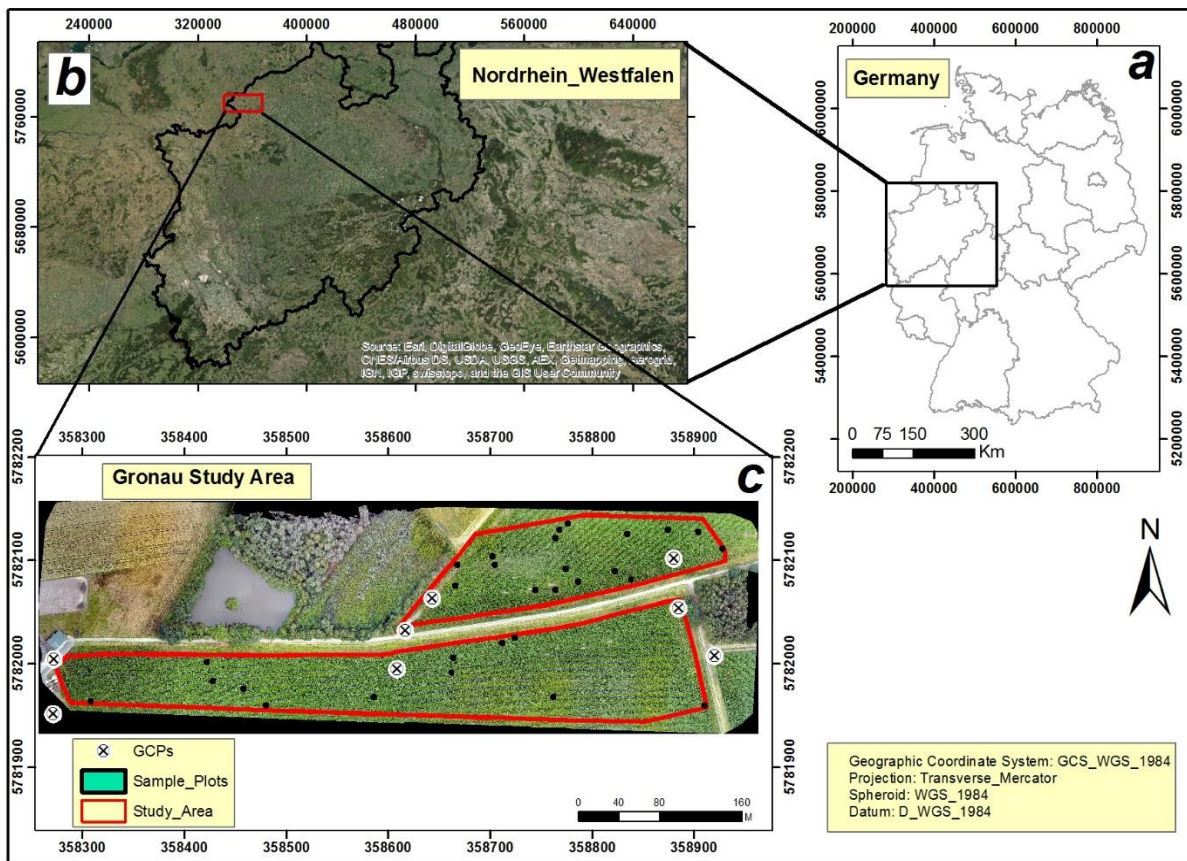


Figure 1: The location map of the study area in Gronau, Germany: (a) Germany Administrative boundaries (provinces); (b) boundary of North Rhine-Westphalia province with Base map world Imagery; and (c) UAV Ortho-mosaicked RGB image, acquired on 08-July-2016.

In this area, maize crop (*Zea Mays L.*), also known as corn, is one of the most cultivated summer cereals along with wheat. It has an important source for a diverse range of applications, like Human diet and mostly in this area for animal feeding. The boundary of the study area was digitized to the extent of the coverage of the UAV images. And then computer based random points were generated in ArcGIS within the boundary of the study area. The study area had two maize fields and 20 random sample points for each and 40 points in total was generated in these two fields (fig.1c). A 2m by 2m area, for field measurement, was taken as a sample plot for each sample point generated at the center and within these sample plots.

2.2. Data and Materials

Data acquired from Unmanned Aerial Vehicles (UAVs) with RGB spectral bands were used in this study. The images were taken at different dates during the Maize growing season from May to September 2016. The main focus of this study was monitoring crop development during the growing season by extracting different image characteristics like Vegetation indices (based on RGB bands) and Crop Surface Models for estimating plant height and yield. The following sections describe the basics of UAVs and data acquisition technics.

2.2.1. Materials and Software used

Several types of equipment and field instruments were used to collect fieldwork data like plant height, the biomass of maize, measuring GCP points and image acquisition. The field instruments used in this study include; UAV, Tablet SAMSUNG, Handheld GPS, Leica GPS, Measuring Tape (3m), meter stick, clipboard, and data recording sheet. The detailed list of materials and different software and their usage is listed in the table below;

Table 1: List of Fieldwork materials and software

Instruments	Purpose
Unmanned Aerial Vehicles (UAVs) (Phantom 4)	Image Acquisition
Leica GPS	Measure GCPs and CPs
Tablet (SAMSUNG)	Display the study area and navigate offline with Locus free
Measuring tape (3m)	Measure plant height at the sample plots
GPS	Measuring/Checking the location of the plots in the field
Clipboard	For holding the recording sheet
Field recording sheets	Record field measurement
Software	
Pix4Dcapture	Mobile application for flight planning for image acquisition.
Pix4D	UAV image processing, to generate DSM and Ortho-mosaic image
ArcGIS 10.4.1	Different GIS activities, preparing maps and layout and processing data that are obtained from Pix4D software
ENVI 5.3 and QGIS 2.18.0	For calculation of vegetation Indices
MATLAB R2016a	For threshold selection for mapping FVC
Microsoft Excel 2010	Statistical Analysis
Microsoft Word 2010	Thesis and report writing

2.2.2. Unmanned Aerial Vehicle (UAV)

The UAV platform used in this study is a phantom-4 (Fig. 2a) which has a stabilized camera model of CanonEOS600D_3.6_4000x3000 mounted on it. The camera has a focal length of 3.722 mm and produces images in visible spectral bands (RGB bands) that are specifically suitable for studying vegetation. The image resolution (Pixel size) at the typical flying height of 50m is 2cm/pixel. The UAV has a payload limit of about 1.5kg and with full payload has a flight duration of around 30 minutes, so due to the low endurance, the whole study area was covered in two to four different flights (table 2). In this study, a single flight at a 50m flying height above the ground had a coverage area of about 7 hectares and produce about 200 images under

standard operation condition. A larger area can be obtained by multiple flights or by increasing the flight height but this will reduce the spatial resolution.

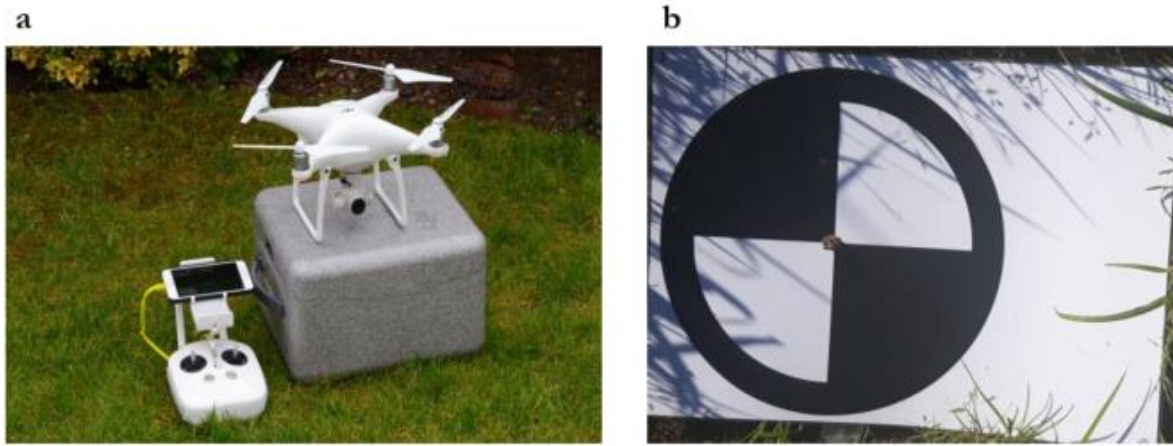


Figure 2: (a) UAV Phantom 4 mounted with RGB bands along with its controlling mechanism (Source: www.dji.com) and (b) Artificial marks for Ground Control Point (GCP) measurement.

2.2.3. Flight planning and UAV Data Acquisition

The first step in UAV image acquisition is preparing the flight plan, using mobile app. Pix4Dcapture software, on the desired area of study. During the flight, the camera was set with the predefined flight plan mission with the desired shutter speed to ensure the best coverage of the area and not being affected by the motion of the UAV and then the images were collected based on the flight plan. These operations were done by the ITC staffs. The UAV is equipped with onboard Global Navigation Satellite System (GNSS) which provides only rough positions; therefore, before flying the UAV artificial marks were placed on the field which had to be visible on the images and were used as Ground control Points (GCPs) and Check Points (CPs) during the image processing for orthophoto creation. These artificial marks were made of 0.3x0.4m (A3) laminated paper (fig. 2b). Those GCP positions/marks were measured using Leica GPS with an accuracy of less than 2cm. Several flights at different dates were carried out on the field with the sensor mounted in nadir position with constant orientation and flying height. The images were collected between 9:30 a.m. to 12 p.m. during the maize growing season from May to September 2016 in every 10 to 15 days interval (table 2).

Table 2: UAV-image data acquisition periods and Number of images acquired.

Day of UAV flight	Date of Acquisition	Number of Images	Flight Height (m)	Area Covered (ha)
1	26 May 2016	One flight (21)	100	8.5636
2	07 June 2016	Three Flights (58)	50	14.0676
3	16 June 2016	Four Flights (98)	50	10.5848
4	08 July 2016	Two Flights (515)	50	14.2974
5	27 July 2016	Two Flights (457)	50	14.0698
6	09 August 2016	Two Flights (449)	50	13.635
7	18 August 2016	Two Flights (441)	50	13.8255
8	08 September 2016	Two Flights (386)	50	14.0411
9	20 September 2016	Two Flights (386)	50	12.8614

The first set of aerial imagery acquired on 26 May 2016, taken at a flight height of 100m over the whole study area with one flight plan and not consistent with the later flights, was excluded from this study. The images were taken from orthogonal view, known as nadir position and a series of overlapped images were acquired during each flight date over the entire study area. On each flight, the imagery had an overlap of 80% forward and 60% side-lap to cover the whole experimental field in two –four flight missions and to allow correct mosaicking of the images to generate a complete orthophoto of the whole study area. This overlap helps in detecting and matching key points from individual photos and also compensate wind disturbance and GPS errors. Examples of raw images taken during the early growing stages are shown in Figure 3 below.



Figure 3: Example of raw images taken by the UAV on June 07, June 16 and July 08, 2016

2.2.4. Maize Development stages

The study of crop growth development stages and quantifying vegetation fraction within a crop field is a first and crucial step prior to investigating further objectives. Monitoring the temporal and spatial variations in vegetation fraction and obtaining information in growth development stages of field crops has many agricultural and ecological importance and is helpful in analysing the relationship between the crop growth processes, agro-meteorological conditions and estimation of phenological and physiological status of vegetation (Yu et al., 2013; J. Torres-Sánchez et al., 2013). Knowing the growth stages of maize throughout the growing season allows the farmers for efficient and timely management on their field. According to Biologische Bundesanstalt, Bundessortenamt und Chemische Industrie (BBCH), Ransom, (2013) and Meier, (2001) describe the maize growth development stages as shown in figure 4 below.

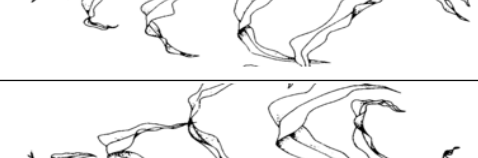
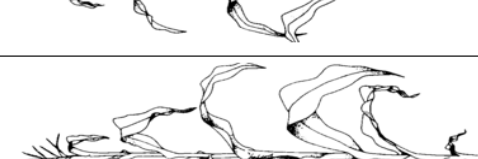
Growth Stages	Vegetative						Reproductive			Maturity
	Emergence	Stages 1&2	Stages 3&4	Stage 5	Stage 6	Stage 7	Stage 8			
Maize development (Ransom, 2013; Meier, 2001)										
	UAV Imagery	07-Jun	16-Jun	08-Jul	27-Jul	09-Aug	18-Aug	20-Sept		
PH Measurement	-	-	-	-	-	13-to-17-Aug	15-to-23-Sept			
Yield Measure.	-	-	-	-	-	-	-			

Figure 4: Maize growth development stages along with the UAV image acquisition dates and field Plant height and Biomass measurements.

3. METHODOLOGY

3.1. UAV Data Processing

The processing of the data/images was carried out using Pix4D- Software, which allows the multiple images that were taken by the UAVs to create digital 3D model, and a mosaicked orthophoto with true RGB color and Digital Surface Model (DSM) was generated. For geo-referencing, the mosaicked image the GCPs were identified manually on each photo and were assigned to the coordinate position which was measured by the Differential GPS. The overall workflow of data processing is presented in Fig.5.

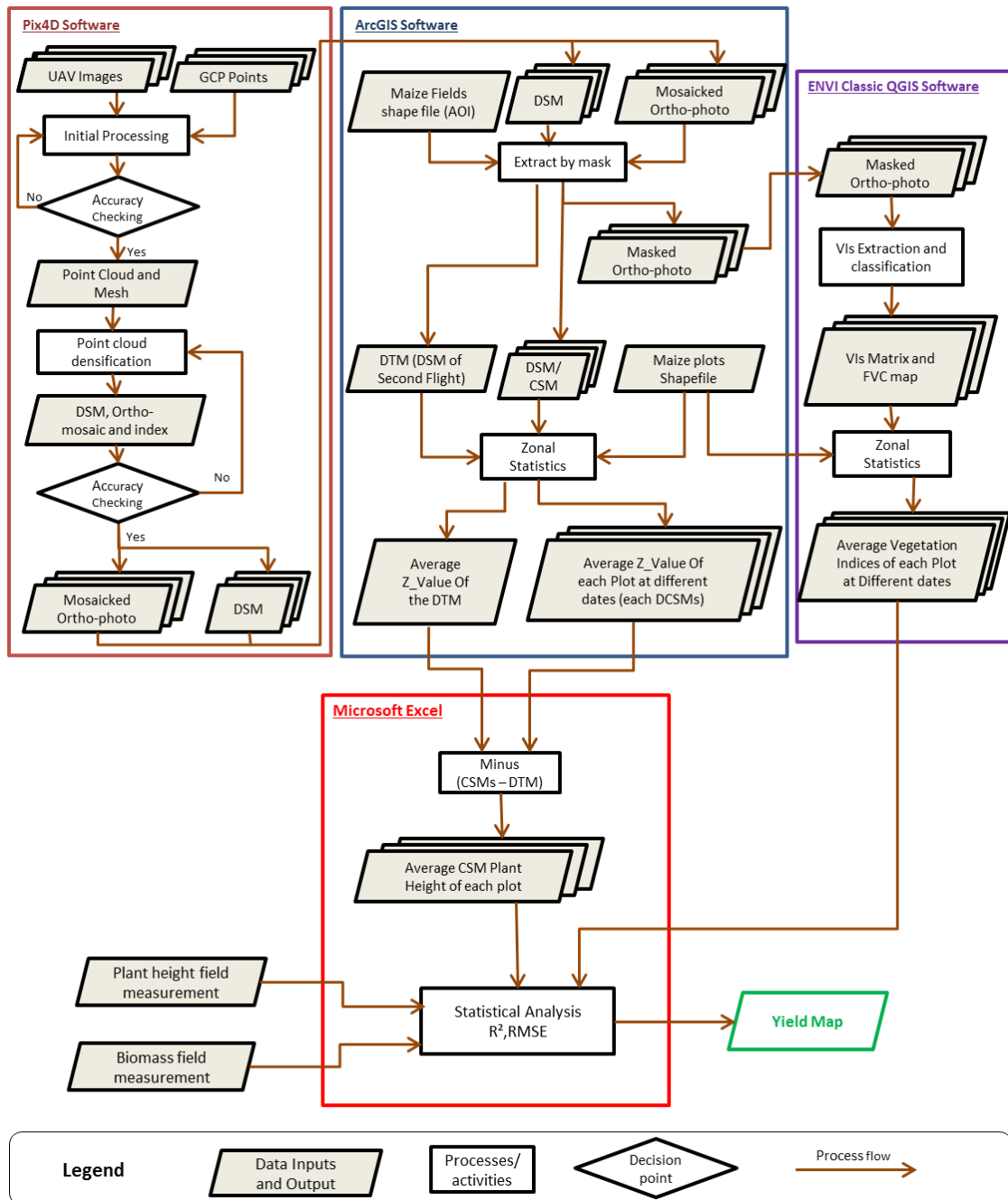


Figure 5: Flow chart showing image pre-processing in Pix4D software for the generation of Digital Surface Model and Mosaicked Orthophoto, and further analysis in ArcGIS, ENVI classic and Microsoft excel.

3.1.1. Image Pre-processing

UAV acquired images were processed to generate Digital Surface Model (DSM) and Ortho-mosaicked image using Pix4D Software for every flight. After the images are acquired they are imported into the software for pre-processing, Figure 6a shows the camera positions (red dots) and flight routes (green line) over the study area. This software allows converting hundreds of images taken by the UAV into geo-referenced 3D surface models (DSM) and 2D Ortho-mosaic image and point clouds which are very interesting outputs for this study. In order to generate DSM/DTM initially camera internal and external calibration and image orientation has to be performed successively (Nex & Remondino, 2014). To generate DSM and Ortho-mosaic, the following three main steps were performed (fig. 6b).

Initial processing: This process allows calibration of cameras (Internal and external camera optimization), extracting and matching key points from individual images (these matching points help to generate 3D points), Geolocation using GCP points and quality report generation (PIX4D Support Site, n.d.). The quality report generated during the processing is presented in appendix 2.

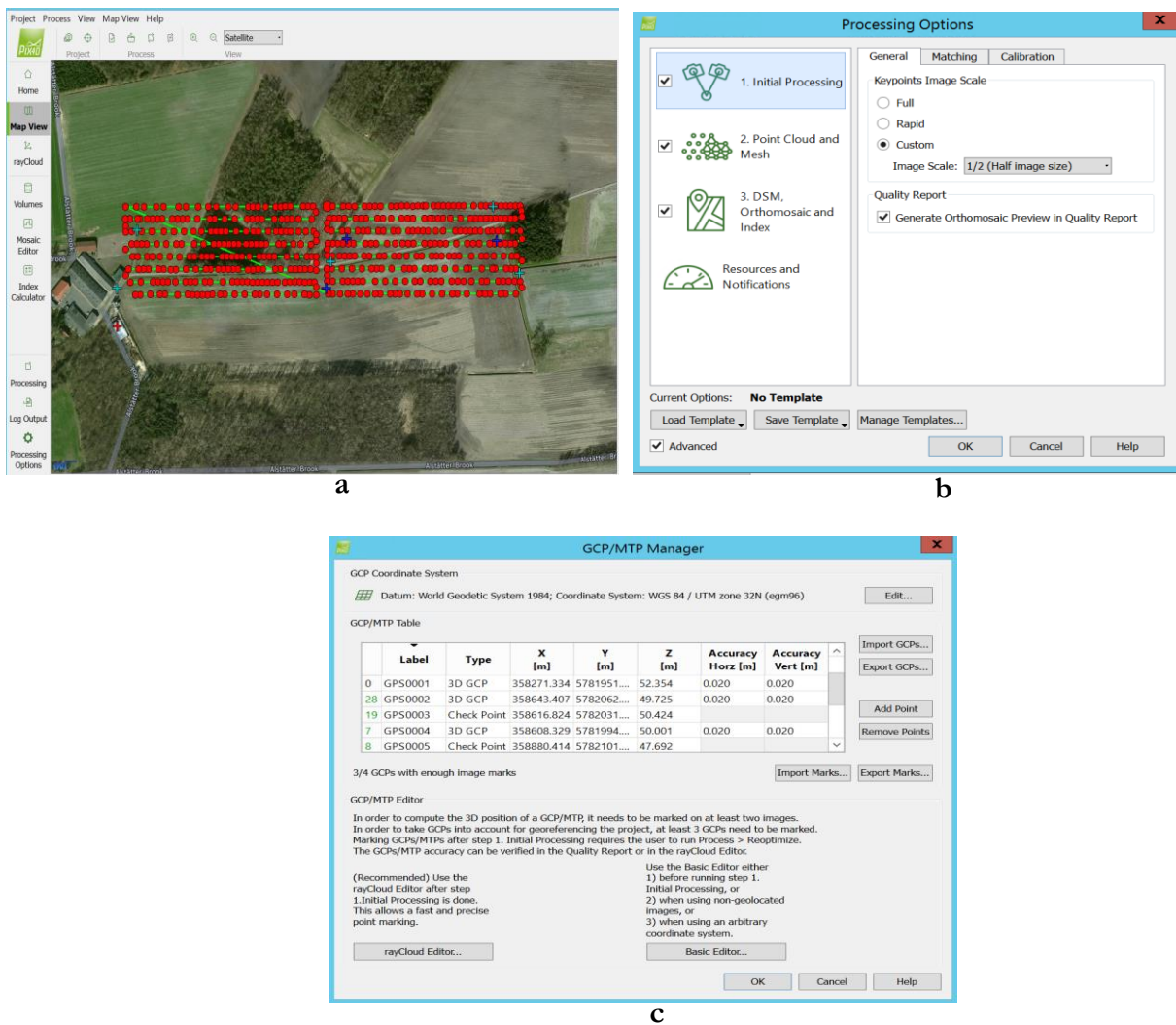


Figure 6: Image processing in pix4D for generation of DSM and Ortho-mosaic; (a) camera positions along with flight route; (b) steps of processing options; and (c) GCP manager for importing GCPs to geo-reference the image.

The GCPs were used in the initial processing phase to locate the photogrammetric images into its true coordinate system. And these GCP points were imported through GCP/MTP manager tool of the software (fig. 6c). Mesas-Carrascosa et al., (2015) described the Pix4D processing steps into 4 phases like (1) aerial triangulation; (2) DSM generation; (3) rectification of individual images; and (4) ortho-mosaic. During the processing, the GCPs help (i) to minimize possible image deformation and possible systematic errors (ii) to avoid instability of bundle solutions and (iii) helps to determine correct 3D shape (Nex & Remondino, 2014).

Point cloud and Mesh: This process helps to increase the density of the 3D points which are computed in the initial processing, and this point cloud densification increases the accuracy of generating DSM and Ortho-mosaic image. This process uses the automated dense image matching techniques which are able to search and match more accurately matching points on the image (that is the point clouds with calculated optimal internal and external camera parameters) which results in more accurate and dense point clouds. Dense image matching technique also helps in extracting dense point clouds and defines the surface of the objects (Nex & Remondino, 2014). The output of this process is normally the 3D sparse or dense point clouds as shown in Figure 7a&b.

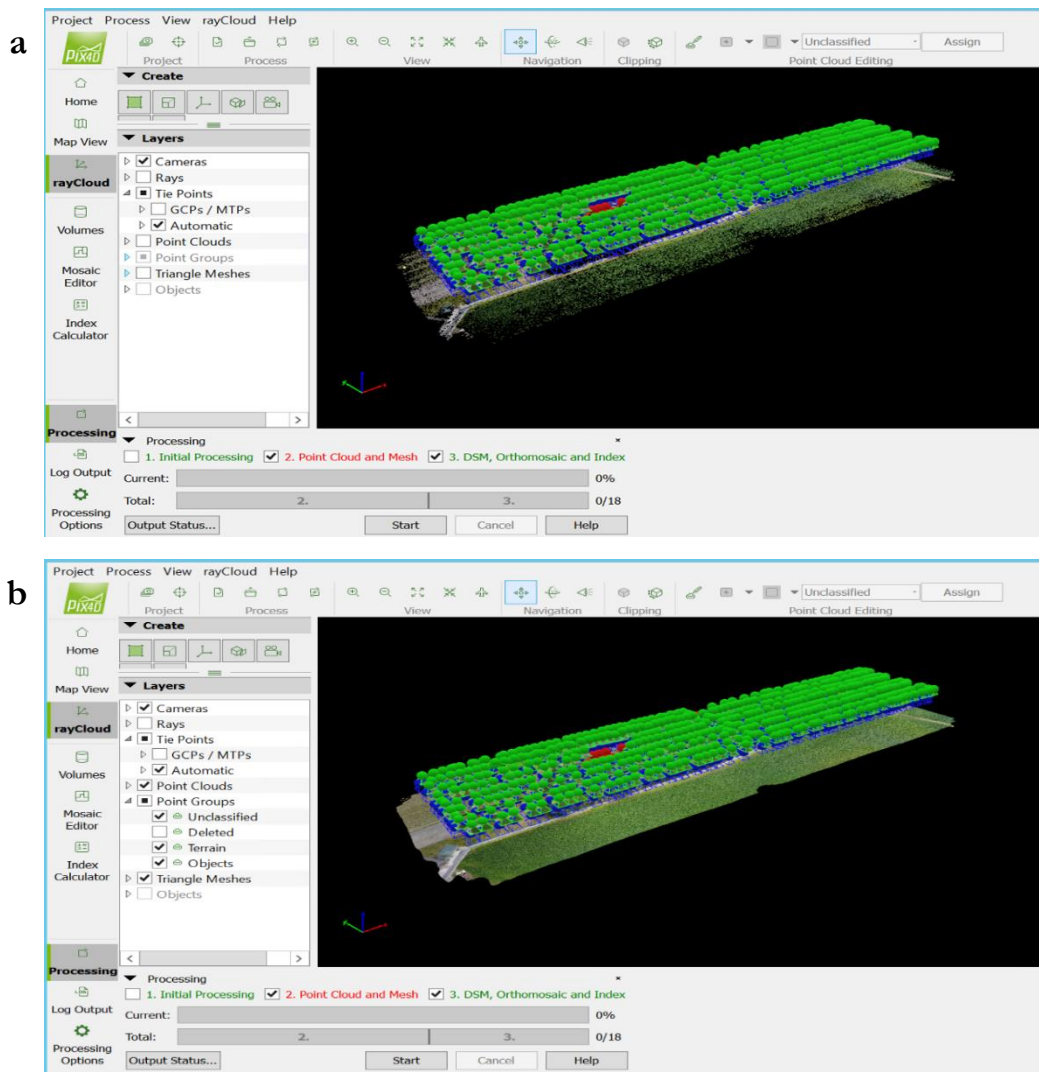


Figure 7: Screen shot of camera positions and geo-located images; (a) Automatic tie points and point cloud; (b) densified point cloud and mesh

DSM, Ortho-mosaic, and Index: In this process a 3-band (RGB) multispectral Ortho-mosaicked image (Fig. 8a) and Digital surface models (DSM) (Fig. 8b) with high spatial resolution (2.25 cm). These two products of this process are the main data requirement for this study, which was generated and exported in *.tiff format. And these outputs were used for further analysis to meet the objective of this study.

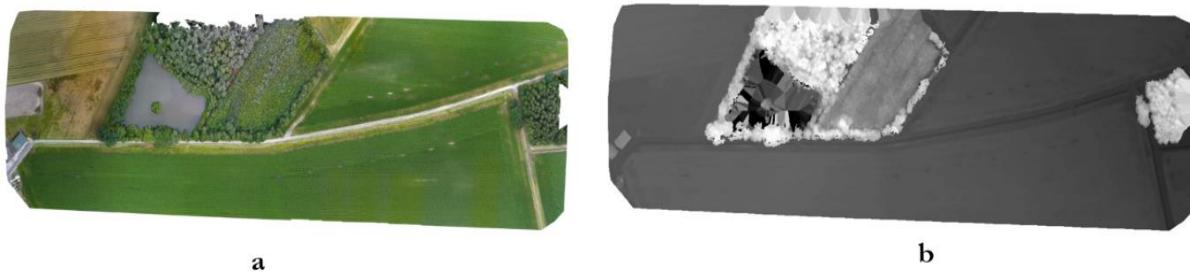


Figure 8: Final output of Pix4D; (a) Ortho-mosaicked image; and (b) Digital Surface Model (DSM)

3.1.2. Generation of Mosaicked Orthophoto and Crop Surface Models (CSMs)

During the second flight the crops were at emerging stage, which means the farms were bare, so the UAV image acquisition during this time (07-June-2016) was used for the generation of the Ground Model. As shown in Figure 9 the generated DSM of each date was later used as Crop Surface Models (CSMs) which was subtracted from the DSM of the second flight, as a reference Ground Model for the rest of the flights as well, for the estimation of the crop height. In addition, mosaicked image (Orthophoto) was generated and exported in a *.TIFF image format for visible band vegetation indices calculations. Grenzdörffer, (2014) presented two different approaches for determining crop heights, that is the Difference method and 3D-point cloud methods. The difference method was applied in this study.

As shown in Fig. 9 comparison of CSMs at different growing stages helps to determine the crop growth development and estimation of plant height (Juliane Bendig et al., 2013). Hoffmeister et al., (2010) and Tilly, (2015) has already introduced the concept of generation of Crop Surface Models using Terrestrial Laser Scanning (TLS) data. In addition to this (Juliane Bendig et al., 2014) demonstrated the estimation of biomass of barley by using Crop Surface Models (CSMs) derived from UAV images.

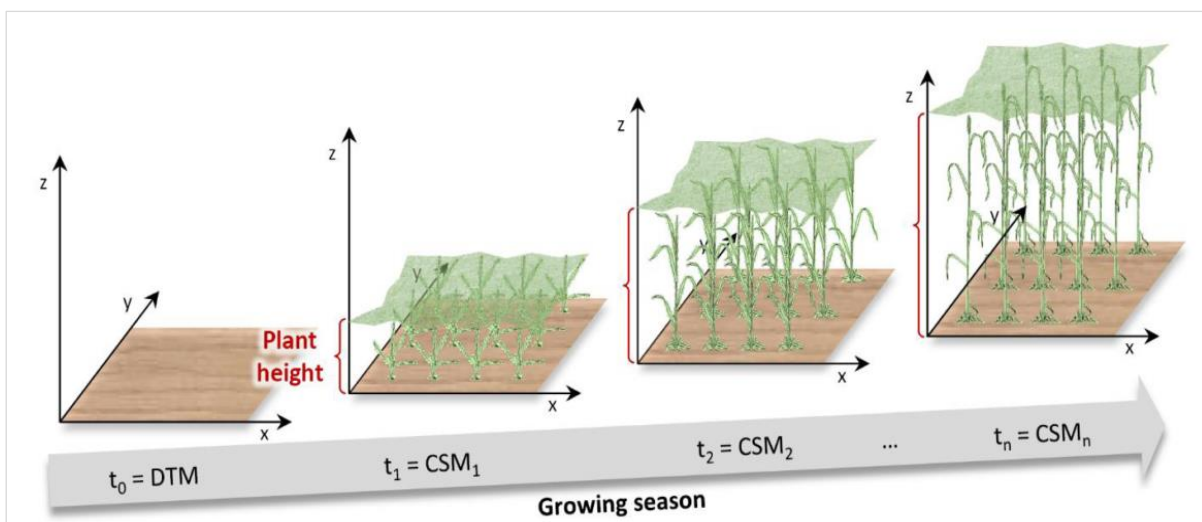


Figure 9: Multi-temporal crop surface models (CSMs) at different growing stages (Nora Tilly, 2015).

Further processing was carried out in Esri ArcGIS 10.4.1. The CSMs of each date was masked by the polygon shape file of the two maize farms, which form an area of interest (AOI). In the next step for each of the 2m x 2m plot, an average elevation (Z_{value}) was calculated from the CSMs of each date using zonal statistics tool to obtain a table with mean elevation and exported as dBase table which can be used for further statistical analysis. To get information on the average plant height of each plot, the CSMs of each date was subtracted from the ground model (DSM of the second flight).

3.1.3. Spectral Vegetation Indices (VIs) Extraction

Spectral vegetation indices were calculated based on the UAV-RGB images. The computed vegetation indices were listed in table 3. These vegetation indices, which provide a powerful indication for the quantification vegetation fraction, were used to classify green vegetation pixels in the mosaicked Orthophoto (detailed description is presented in chapter 4, section 4.1). The choice of these vegetation indices was considered based on the use of RGB bands of the electromagnetic spectrum of the sensor, indices that have been used mainly on crops like maize and the computation algorithms applied includes ratio, summation or band difference. Based on these UAV-images of RGB spectral bands six vegetation indices were calculated by ENVI (using band math tool) and QGIS (using Semi-Automatic Classification Plugin, **SCP**) software. Then At each growth stage, average vegetation indices for each plot were extracted using 'zonal statistics as table' tool in ArcGIS to calculate the average vegetation Index value for the entire plot. And the process is repeated for each vegetation indices obtained at different dates.

Table 3: The vegetation indices computed based on visible spectral bands.

Item	Equation	Source
Excess Green VI (ExG)	$2G - R - B$	(Woebbecke et al., 1995) as cited in (Li et al., 2016)
Color index of vegetation (CIVE)	$0.441 * R - 0.881G + 0.385B + 18.78745$	(Kataoka et al., 2003)
Vegetativen (VEG)	$G/R^a B^{1-a}$ with $a=0.667$ as in its reference	(Hague, Tillett, & Wheeler, 2006)
Excess green minus excess red (ExGR)	$ExG - 1.4R - G$	(Camargo Neto, 2004) as cited in (Li et al., 2016)
Normalized green-red difference index (NGRDI),	$(G - R) / (G + R)$	(Gitelson et al., 2002)
Combination (COM)	$0.25ExG + 0.3ExGR + 0.33CIVE + 0.12VEG$	(Guijarro et al., 2011)

3.1.4. Computation of Fractional Vegetation Cover (FVC)

The above-mentioned vegetation indices provide a powerful indication for the estimation of vegetation fraction (J. Torres-Sánchez et al., 2014). Figure 10 below shows an example mapping Fractional vegetation cover map, using ExG vegetation index, which is presented in the study of Geipel, Link, & Claupein, (2014).

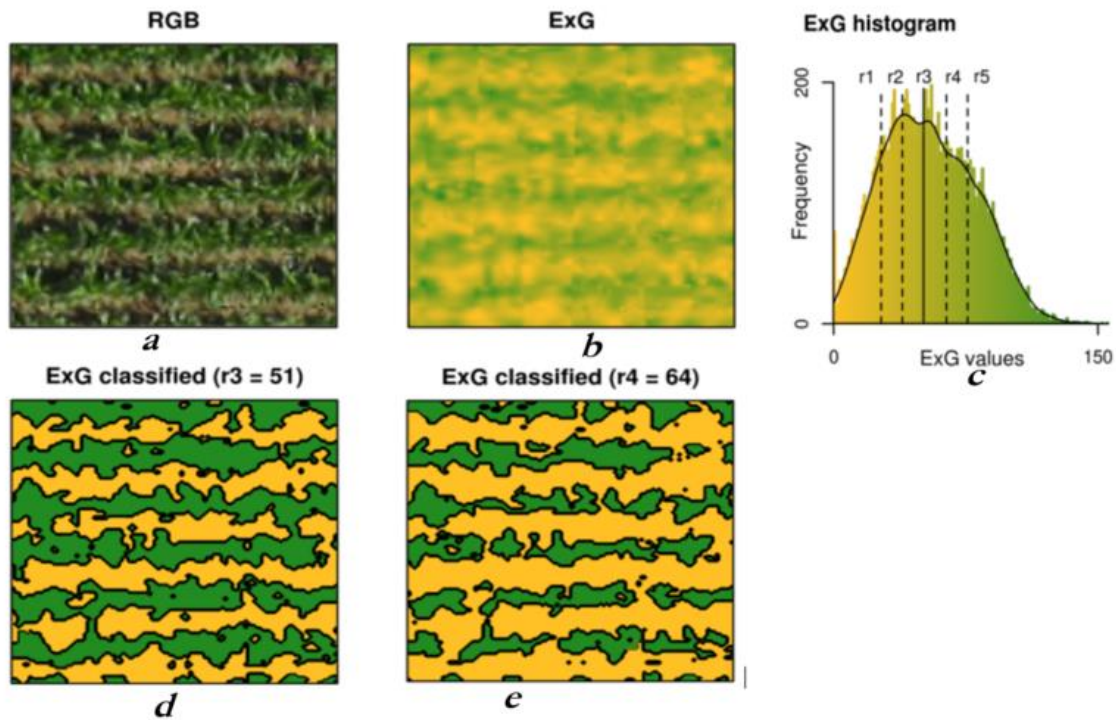


Figure 10: (a) True color image; (b) ExG Image; (c) ExG histogram with the different thresholds (r1 – r5); and (d&e) classified images with different thresholds (green vegetative and yellow non-vegetative) right after applying VIs and threshold to differentiate vegetative and non-vegetative pixels.

Fractional vegetation cover (FVC) was quantified by classifying green vegetation pixels based on the six Vegetation Indices (Vis) calculated from UAV-RGB spectral bands of the Orthophoto which was obtained from the Pix4D (equ.1). These VIs are used to convert the original RGB-image with three spectral bands to a greyscale single band. All the mosaicked orthophoto obtained from different flying dates were transformed to a greyscale by the application of the above-mentioned vegetation indices. These greyscale images were then converted to a binary image by classifying the image using the prefixed threshold, pixels values greater than the threshold were classified as vegetation whereas those pixels lower than the threshold were classified as soil. In grayscale image processing, it is important to select adequate threshold level to identify objects from their background (OTSU, 1979). The threshold was selected based on the Otsu thresholding method algorithm using Matlab. Once the image pixels were classified percentage of vegetation cover was quantified to determine FVC.

For verification, the RGB-image was also classified to vegetative and non-vegetative parts using supervised classification by a set of points located on vegetation and non-vegetation (Soil). These points were used as training points to estimate the real percentage of the ground covered by vegetation, and later these were compared with the FVC computed from the vegetation indices as shown in table 4. The ground is fully covered by vegetation from first of august. In the study of J. Torres-Sánchez et al., (2014) used the expressions (1) and (2) for calculating the percentage fractional vegetation cover and classification accuracy respectively.

$$\text{FVC} = \left(\frac{\text{Number of Pixels Classified as Vegetation}}{\text{Total Number of Pixels}} \right) * 100 \quad \dots\dots\dots (1)$$

$$\text{Classification Accuracy (\%)} = 100 - |(\text{OVF}-\text{VF})| \quad \dots\dots\dots (2)$$

Where FVC/VF = Fractional Vegetation Cover in percentage and OVE = observed vegetation fraction, in this case, the classified RGB image.

3.2. Field Data Collection for Height and Biomass

The simple random sampling method was used in this study and typically mature maize plant has the leaves, the stalk and the node (the point at which the leaf joins the stalk). This structure makes it difficult to the manual survey on the ground and Anthony et al., (2014) defined the height of maize plant as the distance from the top node to the ground. Field measurements, mainly plant height, and biomass measurement, on the selected sample plots were done using a tape and weighing balance respectively. Manual plant height measurement was taken at two different growth stages, one was during tasselling which corresponds to UAV flight seven (18-Aug-2016) and the second was at physiological maturity (just before harvesting) this also corresponds to UAV flight nine (20-Sep-2016) but biomass measurement was taken only at maturity just before harvest time.

The plant height (PH) measurement was taken randomly from five maize plants for each plot manually. The mean plant height for each plot was calculated by averaging the measured plant heights. After reaching physiological maturity, the five randomly selected maize plants were harvested by cutting the whole plant from the bottom of the ground for each plot. The harvested maize plants were weighed in the field using the weighing balance to record the fresh biomass of the plants.

Twenty plants from different plots were transported to the laboratory for the dry biomass analysis. Finally, these plants were dried at 105°C until their mass reached a constant weight (48 hours). In our study area, the crops were planted at a row spacing of 0.75 m and interplant spacing of 0.15 m and the average plant density per square meter was found to be 10. Therefore, the Above Ground Biomass (AGB) in kg/m² for each plot was calculated as the product of the dry weight per plant (kg/plant) and the average plant density (number plants/m²) which was determined by the interplant and line/row spacing (m).

3.3. Statistical analysis

Statistical regression analysis was carried out in Microsoft Excel 2013. Different regression models were used to estimate the total biomass of the crops at the end of the growing season using image characteristics like the height derived from Crop Surface Models (CSMs) and vegetation indices of the mosaicked orthophoto of different growing stages of the whole growing season.

Exponential regression analysis using maize dry biomass which was collected at the physiological maturity as the dependent variable and plant height measured at the field right before harvesting as an independent variable were fitted in an exponential growth model ($Y = a * \exp^{bx}$) to access the relationship between the maize yield (biomass) and plant height. Determination coefficient (R²) was used to evaluate the strength of the relationship between Above Ground Biomass (AGB), (fresh and dry biomass), and Plant Height (PH).

In this study, linear and exponential regression equations were also used in describing the regression relationships of Vegetation Indices versus above ground biomass (dry and fresh) and plant height versus biomass respectively. In addition to this, stepwise multiple linear regression equations were used to estimate

fresh/dry biomass using the combined parameters of vegetation indices and plant height derived from the UAV images. The maize Fresh and dry biomass, as well as height regression models, were evaluated by the Coefficient of determination (R^2) and Root Mean Square Error (RMSE) and percentage normalized Root Mean Square Error (nRMSE). RMSE is related to the magnitude of the observed variables, while nRMSE is a normalized value that can be used to compare the performances of different regression models. A lower nRMSE often indicates a better regression performance. RMSE and nRMSE were calculated using equation 3 and equation 4 respectively (Li et al., 2016):

$$RMSE = \sqrt{\sum_{i=1}^n \frac{(Y_i - Y'_i)^2}{n}} \dots\dots\dots (3)$$

$$nRMSE = \frac{RMSE}{Y_{max} - Y_{min}} * 100 \dots\dots\dots (4)$$

Where n is the number of observations, Y_i is the observed values, Y'_i the predicted values, Y_{max} and Y_{min} are the maximum and minimum observed value.

4. RESULTS AND DISCUSSION

4.1. Vegetation Indices and Fractional Vegetation Cover (FVC)

Six Vegetation Indices were tested in mapping Fractional Vegetation Cover (FVC) by comparing with the classified ortho-mosaicked images. As described in section 3.1.3, these vegetation indices were calculated from fine spatial resolution RGB images acquired by the UAV. The whole study or the maize farm area reached near 100% vegetation cover by the end of July-2016. That means vegetation indices obtained from the first four flights(from early June to late July) were helpful in mapping FVC whereas the rest flights that were taken on and after August had no importance for FVC mapping since the ground was totally covered by vegetation during this period. These vegetation indices were used for classifying green vegetation pixels in the mosaicked images and quantify the vegetation fraction.

The vegetation indices (VIs) were first stored in 8bit unsigned with pixel values ranging from 0 to 255 and based on Otsu method discussed in chapter 3, thresholds were selected to differentiate the vegetation from the background (soil). And the result of this study showed that the predefined thresholds for each vegetation indices are ExG = 110, CIVE = 125, VEG = 90, ExGR = 130, COM = 110 and NGRDI = 90. And the images of the six vegetation indices were classified based on a pre-defined threshold into two classes vegetation and non-vegetation (soil) as shown in appendix-1a and 1b.

The thresholds were evaluated and cross-validated with FVC extracted from supervised classification method of the RGB image. As shown in the Table 4 out of the six vegetation indices tested in this study two best vegetation indices (ExG and COM) were selected considering their classification accuracy along with the first four temporal series, for better vegetation cover mapping with classification accuracy ranging from 94.52% to 99.16% for ExG and 91.45% to 96.94% for COM.

Similarly, J. Torres-Sánchez et al., (2014) studied eight vegetation indices (the Six vegetation Indices which were studied in this paper and two additional VIs, Woebbecke Index (WI) and one combination VI) for mapping vegetation fraction based on RGB images for wheat crop. They found ExG and VEG indices are best in vegetation fraction mapping with the accuracy ranging from 83.93% to 87.75% for ExG, and 83.74% to 87.82% for VEG at 60 m flight height with spatial resolution of 2.28 cm. Higher accuracy is observed in our result, the reason could be the crop that is maize in our case can easily be distinguished from its background when compared with wheat. This is because the maize plants were sown with definite row and interplant spacing and had larger leaves whereas wheat is scattered by broadcasting which made the classification accuracy lower.

Table 4: Percentage vegetation fraction, the selected threshold and classification accuracy of each vegetation indices obtained from the Ortho-mosaic at 07-June, 16-June, 08-July, and 27-July.

Date	Area covered by vegetation in percentage												
	Classified Ortho-mosaic	Vegetation Indices/Thresholds											
		ExG		CIVE		VEG		ExGR		COM		NGRDI	
		Tresh=110	Classification Accuracy	Tresh=125	Classification Accuracy	Tresh=90	Classification Accuracy	Tresh=130	Classification Accuracy	Tresh=110	Classification Accuracy	Tresh=90	Classification Accuracy
7-Jun-16	11.97	15.44	96.53	14.51	97.46	1.1	89.13	9.13	97.16	3.42	91.45	11.2	99.23
16-Jun-16	37.85	32.37	94.52	43.14	94.71	22.79	84.94	30.71	92.86	44.01	93.84	44.21	93.64
8-Jul-16	93.01	93.85	99.16	58.41	65.4	35.59	42.58	66.43	73.42	97.75	95.26	28.32	35.31
27-Jul-16	94.35	97.8	96.55	65.84	71.49	22.1	27.75	78.06	83.71	97.41	96.94	57.31	62.96

In addition to visible band vegetation indices for mapping Vegetation fraction Cui et al., (2011) found NDVI vegetation index which provides a significant relationship with percentage vegetation cover with a correlation coefficient of 0.710. Furthermore, NDVI regardless of species had also a strong relationship with percentage ground cover with R^2 of 0.87 (Prabhakara et al., 2015).

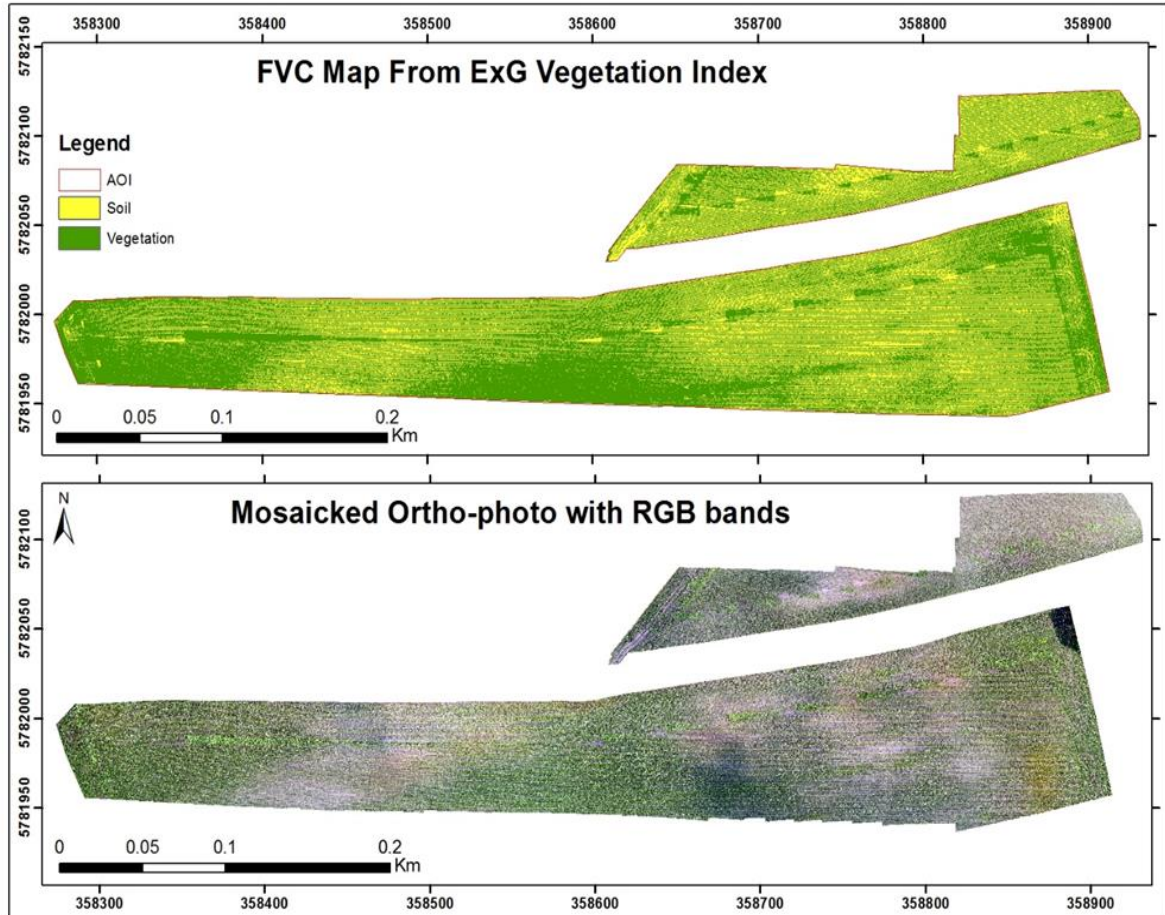


Figure 11: Single band classified image (FVC map) obtained from the ExG vegetation index upper image and Mosaicked orthophoto with RGB bands lower image (16-Jun-2016).

Figure 11 for example, shows the FVC map estimated from ExG vegetation index and mosaicked orthophoto during the early growing stage of the whole maize field of the study area using UAV images acquired on 16-Jul-2016.

Based on the results of this study the hypothesis 1; : There is a significant relationship (correlation) between Fractional Vegetation Cover (FVC) obtained from classified RGB image and vegetation indices calculated from visible spectral bands of UAV images at different growing stages was accepted for ExG and COM vegetation indices during the first four flights, that is from germination Stage (07-Jun-2016) to inflorescence emergence, heading stage (27-July-2016).

In addition to mapping Fractional Vegetation Cover (FVC), the computed vegetation indices were also analyzed in predicting end biomass/yield and plant height at respective growth stages. The result of this study shows that vegetation indices calculated during stem elongation and Inflorescence emergence/heading stage, which is from early July to early August (Fig. 4), have a potential to estimate the height as well as the biomass of the crops. This will be further discussed in detail in the next section 4.3.

4.2. Crop Surface Models (CSMs) for Plant Height Estimation

The average plant height of each plot obtained from CSMs (PH_{CSM}) and field measured plant height (PH_{ref}) was fitted on a linear regression model and the result is presented in a scatter plot along with the regression equation and was analyzed by their coefficient of determination (R^2), RMSE, and nRMSE values. The result showed high correlation between plant height derived from CSMs and field measured plant height with R^2 and nRMSE of 0.68 and 11.65% (on 18-August) and 0.85 and 9.14% (on 20-September) respectively (Fig. 12a&b).

A strong challenge during this study was, the GCP points were not sufficiently distributed over the entire study area especially to the east part of the field. This results in low accuracy of CSM generation on some flying dates (such as flights taken on 27-July, 09-August, and 18-August) which gives unexpected plant height from CSMs in some plots. These plots were removed from analysis to avoid errors aroused from them in estimating fresh and dry biomass. Still, residual errors might be present due to inaccuracy in CSM generation, this could be the reason for a decreased $R^2 = 0.68$ during the seventh flight (on 18-August).

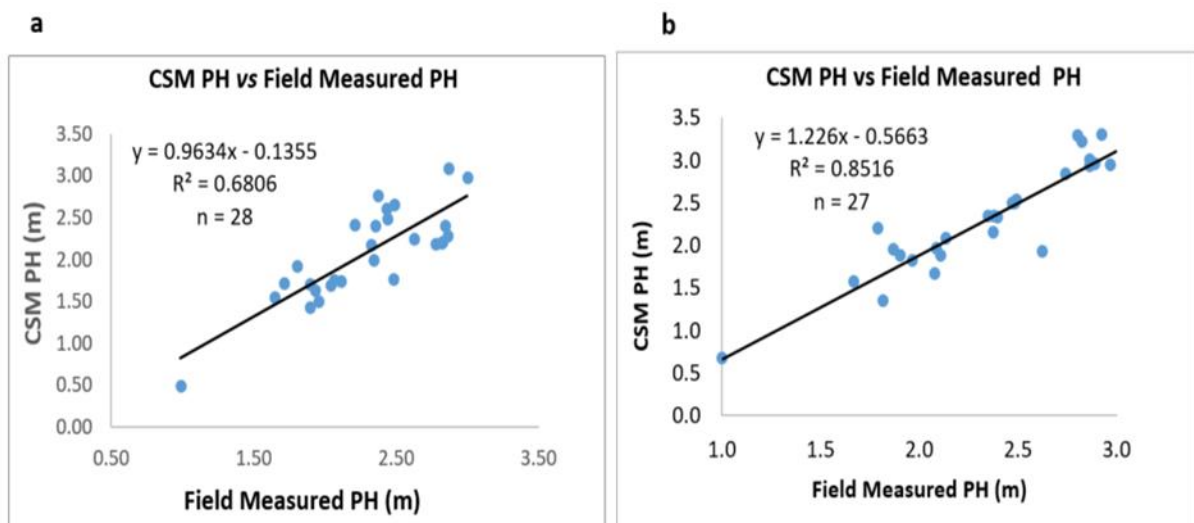


Figure 12: Field measured Plant Height in relation to plant Height derived from CSMs (a) at 18-Aug-2016 and (b) at 20-Sep-2016.

An example of CSMs of two sample dates that are 08-Aug-2016 (a); and 27-Jul-2016 (b) are shown in Figure 13. Dark pink to brownish color indicates low growing areas and light green to dark green areas indicate high plant heights. This height difference comes from excessive water stress (water logging), especially to the east part. In our study area, extreme rainfall was observed especially during late June and July, for example, the maximum precipitation in this area was about 60 mm on 24-Jun-2016. Another reason for the variation crop height could be due to environmental effects such as climatic condition and soil type. Vegetative growth of the crop was similar on the entire field until the end of June, but from this time onwards difference on vegetative growth development was observed within the field which leads to the variation in the end biomass/yield production.

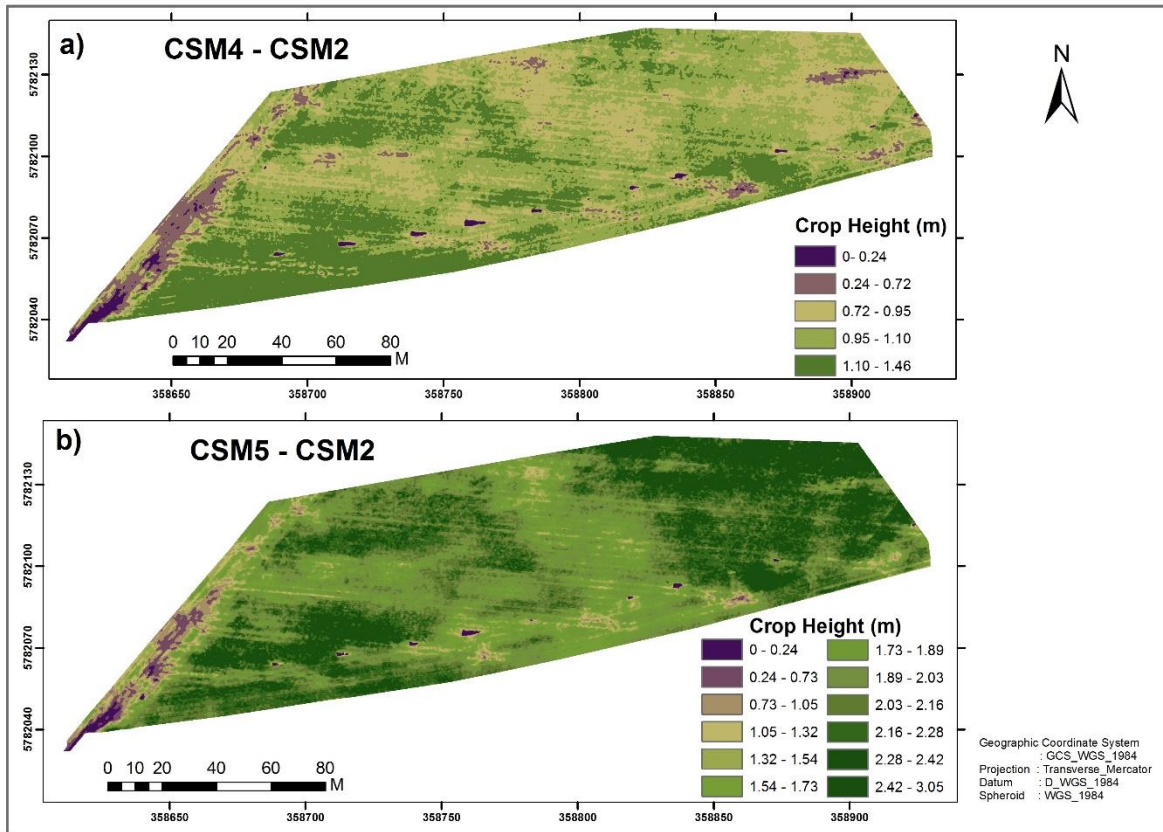


Figure 13: Plant heights from Crop Surface Model of field two (a) during flight_4 (08-Jul-2016); (b) during flight_5 (27-Jul-2016).

Plant height derived from Crop Surface Models (CSMs) from different UAV flights, of selected plots were also plotted on a line graph against time to see the growth development of the crops (Fig. 14). The gray line shows the growth development of maize for sample plot 19, which is very low growing plot, with a maximum height of less than 1m in September. As a result, the yield obtained from this plot was also very low. The orange, light blue, and yellow lines show for plot 2, plot 7 and plot 20 respectively from medium to high growing plots. And the dark blue line indicates the average growth development of the whole field (average of all plots). As indicated by the arrow in Figure 14 unexpected drop in plant height is shown on 18-Aug-2016, this is due to inaccurate CSM generation which results from insufficient distribution of GCP points (as discussed above).

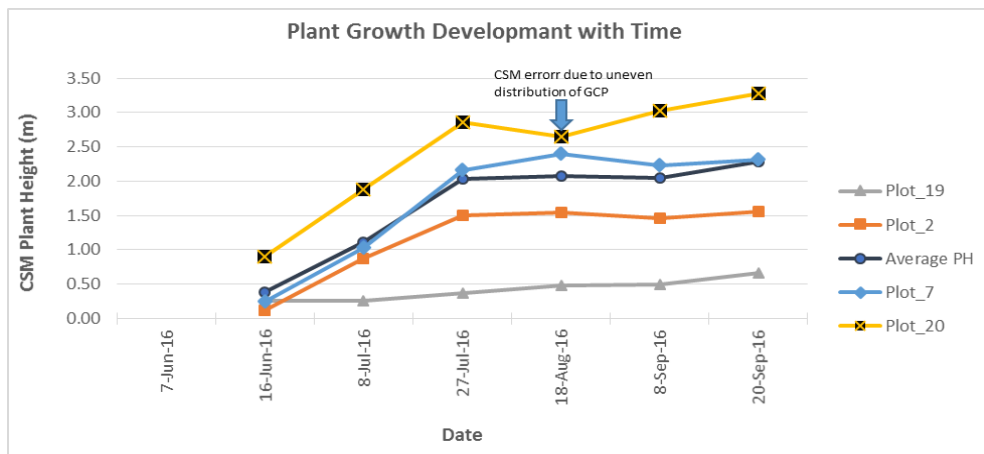


Figure 14: An example of crop growth development of low, medium and high growing plots through time.

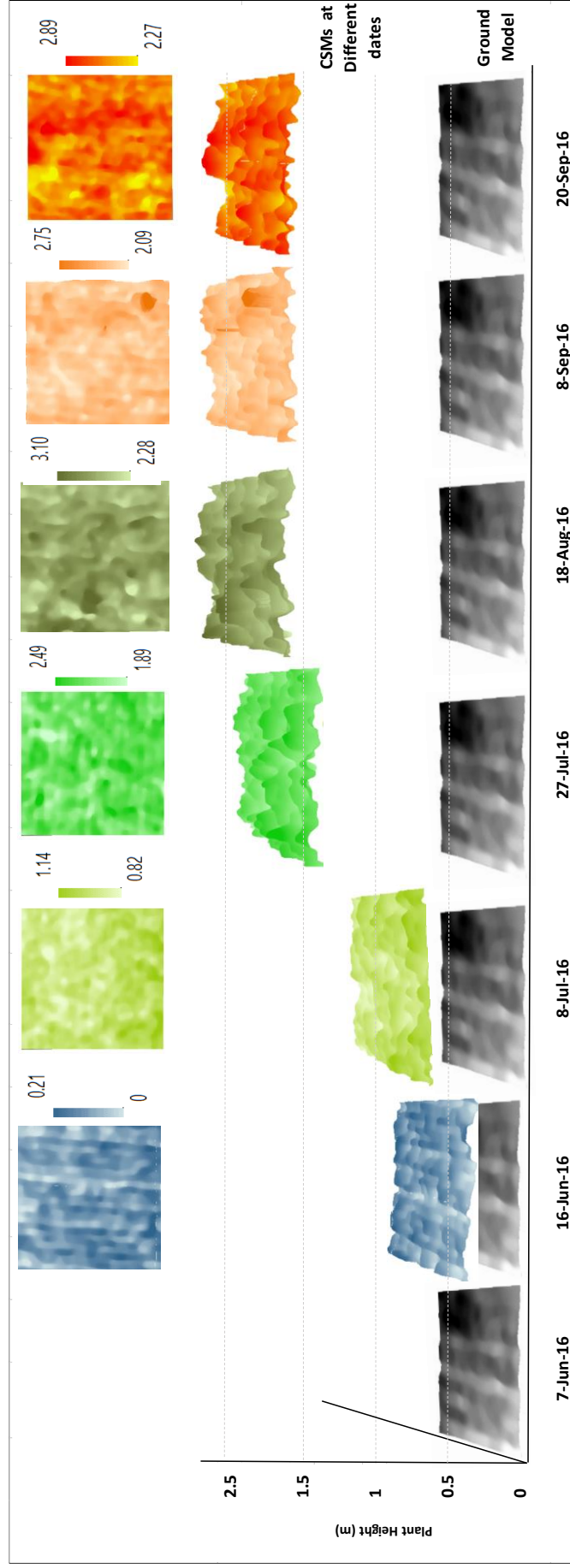


Figure 15: Crop Surface Models (CSMs) at different dates; the gray surface is the reference ground model (obtained from 7-Jun-2016) and the colored surfaces are the CSMs of different (dates from 16-Jun to 20-Sep-2016).

The Crop Surface Models (CSMs), which were obtained from UAV images at different dates, represent the surface of the crops with high spatial resolution (2.25 cm) at different growth stage were used to determine the actual plant height by subtracting from the ground model which was obtained from DSM of the second flight (07-Jun-16) where there were no crops. The gray colored surface represents the ground model and the colored surfaces represent the crop canopy surface (CSMs) at different dates. Figure 15 shows a visualized map of plant height with same spatial resolution with Crop surface Models. Plant growth (spatiotemporal difference in plant height) between two desired dates can also be measured by subtracting CSM of earlier date from CSM of the later date.

As described on the literature review and the results obtained in this study very high-resolution multi-temporal crop surface models (CSMs) were important in determining crop height for growth monitoring and development by a means of low-cost UAV equipment. The images for this study were collected from early June, just before crop germination, to late September just before the date of harvesting. GCPs with sufficient visibility were also collected during each flight (acquisition date) and which were manipulated during data processing. Crop Surface models (CSMs) were generated from Pix4D software for maize biomass estimation using very high-resolution UAV images for monitoring crop growth development. Comparatively, in other studies the Structure from Motion (SfM) based software Agisoft PhotoScan were used to process UAV acquired stereo images for CSM generation to accurately estimate crop height and crop growth monitoring (Juliane Bendig et al., 2015; Geipel et al., 2014; J Bendig et al., 2013; J. V. Bendig, 2015).

Accurate pre-processing of very high spatial resolution data is very important for accurate crop height and Biomass/yield estimation. CSM generation is one of the most important output of pre-processing of fine spatial resolution imagery and its concept includes generating of absolute plant heights as well as monitoring growth development of crops during the growing season (J. V. Bendig, 2015). In the current study, images were collected with sufficient overlap (80% forward and 60% side lap). Similarly, other studies used flight plans with side to forward overlap of 44% to 90% (J Bendig et al., 2013); 60% to 70% (Ruiz et al., 2013); 30% to 60% (Jorge Torres-Sánchez et al., 2013); 50% to 80% at 60m flying height (Mesas-Carrascosa et al., 2015) respectively to generate CSMs for accurate estimation of crop heights.

The accuracy of the CSMs can be affected by different factors like image overlap and the number and distribution of GCP points over the study site. As discussed in section 4.2. the coefficient of determination was 0.68 and 0.85 this is probably due to unevenly distributed GCPs. Enough and well distributed GCPs increase the absolute accuracy of DSM/CSM generation, Juliane Bendig et al., (2014) for example, took 15 GCP point on an area of about 0.2 ha evenly distributed over the study site which is much smaller as compared to our study field around 13 ha with only 7 GCPs and were not evenly distributed. Their result shows high accuracy with R^2 of 0.92 in estimating crop height of barley (which has considerably more homogeneous canopy surface as compared to maize) which was a stronger correlation as compared to the result of this study ($R^2 = 0.70$ during Tasselling and $R^2 = 0.85$ during ripening). This shows substantially higher accuracy of crop heights from CSM can be obtained by using sufficient amount, well-distributed and highly visible GCPs. Similarly, higher correlation was also found by Tilly, (2015) with R^2 of 0.93 for maize and N. Tilly et al., (2013) R^2 of 0.71 for paddy rice using TLS data which was validated by manually measured plant heights.

Based on the results described above crop heights derived from Crop Surface Models (CSMs) of UAV images have high potential in accurately estimating plant height. Hereby we accept hypothesis two; (**H₀**: Crop Surface Models can calculate crop height accurately); provided that there should be sufficient and well-distributed GCP points for accurate CSMs generation.

4.3. Empirical models for biomass assessment at harvest

This study focused on estimation of fresh and dry biomass at harvest using RGB derived vegetation indices and plant height obtained from Crop Surface models (CSMs) of different campaigns of the growing season. The overall objective of this study was to establish robust empirical models for non-destructive crop biomass of maize at field level for monitoring growth development throughout the growing season. Therefore, this study developed linear regression models between VI & Biomass, exponential relation between crop height & biomass and multiple linear regression models with the combined plant height derived from CSMs and vegetation indices and these regression models showed an optimal result.

4.3.1. Vegetation Indices modelling for yield assessment

Crop biomass is an important parameter for efficient crop management during the growing season and yield estimation. Linear relationships were accessed between vegetation indices as the independent variable and biomass (fresh and dry) at harvest as the dependent variable.

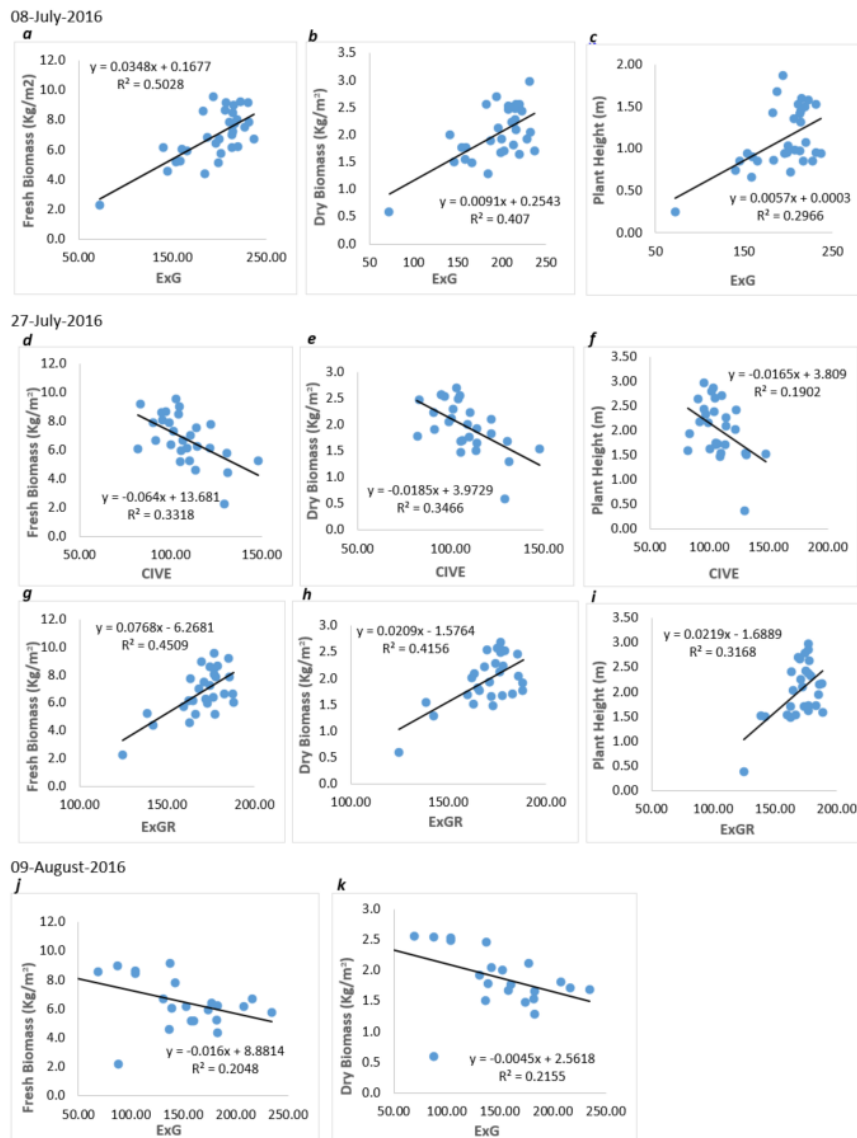


Figure 16: Cross-validation relationships of fresh/dry biomass, height and Vegetation indices of different dates; (08-Jul-16) ExG *versus* biomass and height (**a-c**); (27-Jul-16) CIVE and ExGR *versus* biomass and height (**d-i**); and (09-Aug-16) ExG *versus* biomass (**j-k**).

At 95% confidence level a significant correlation between fresh/dry biomass at harvest time and vegetation indices (such as ExG, CIVE, ExGR, COM, NGRDI) were observed during the vegetative growth stages (Fig. 4). Similarly, correlation with CSM plant heights was also revealed by ExG, CIVE, ExGR, and COM vegetation indices. Basically, all the vegetation indices had low R^2 , ranging from 0.004 to 0.50 but have a significant relationship at $p < 0.05$, to estimate yield at harvest time and crop height at a respective growth stages (Table 5) and in addition to R^2 the RMSE and nRMSE values were used to select the best model for estimation. For the estimation of biomass (fresh and dry) and crop height the ExG, CIVE, ExGR, and COM vegetation indices were fitted to linear regression equations and the rest (VEG and NGRDI) were not significant at 95% confidence level, so they were not included for assessing biomass and plant height. Based on the results from Table 5 and Figure 16, ExG vegetation index had a higher correlation with biomass and height during stem elongation stage (08 July) (Fig.4) with a p-value of less than 0.001, and its correlation declines from late July onwards. During inflorescence emergence and heading stage (27 July), CIVE and ExGR models had better fit with higher R^2 and lower RMSE as compared to other vegetation indices.

As shown in Table 5 and figure 16 the ability of the vegetation indices, predicting the yield at harvest and crop height at different growth stages, was analyzed based on their behavior with respect to R^2 , RMSE, and nRMSE values. On 08-July (stem elongation stage) (Fig.4), ExG had significant relationship with $R^2 = 0.5$ and 0.4, RMSE = 1.2 kg/m² and 0.4 kg/m² and nRMSE = 12.3% and 15.6% for fresh biomass and Dry biomass respectively, and R^2 of 0.3 for plant height at $p < 0.001$ (Fig. 16a – 16c). During inflorescence and heading stage (27-July) ExG, CIVE, ExGR, and COM have significant relationship with biomass and height at 95% confidence level, out of which CIVE with negative linear relationship ($R^2 = 0.33 - 0.35$), and ExGR with positive linear relationship ($R^2 = 0.42 - 0.45$) were better in estimating yield and height with lower RMSE and nRMSE at $p < 0.001$ (Table 5 and Fig. 16d-16i). At flowering stage (09-August) ExG seem to have a significant relationship with fresh and dry biomass at $p < 0.05$ with negative correlation but it was supposed to have a positive relationship, that means from this growth stage it had no importance in estimating biomass (Fig 16j - 16k).

Based on the results obtained at different dates the vegetation indices performs differently with respect to time. That is, ExG vegetation index performed better during stem elongation (08-July) with highest R^2 , Lower RMSE and lower percentage error (nRMSE) in estimating yield and plant height. The CIVE and ExGR vegetation indices during stage 5 (Fig. 4) had also reasonable estimation accuracy next to ExG. The relationship between vegetation indices and biomass were found higher (with an estimation error ranging from 12% - 22%) than those between vegetation indices and plant height (with an estimation error ranging from 18% - 34%) (Table 5). This could be because of the errors occurred from plant height derived from CSMs (PH_{CSM}) as described in chapter four.

Table 5: The regression relationships between fresh and dry biomass, Plant Height derived from CSMs Modelled from different vegetation indices and plant height, where $R^2 =$ coefficient of determination; RMSE = root mean square error and nRMSE = normalized root mean square error.

Date	Independent variable	Fresh Biomass/Yield			Dry Biomass/Yield			CSM Plant Height					
		Regression Equation	R^2	RMSE (Kg/m ²)	nRMS E (%)	Regression Equation	R^2	RMSE (Kg/m ²)	nRMSE (%)	Regression Equation	R^2	RMSE (m)	nRMSE (%)
16-Jun-16													
8-Jul-16	ExG	$Y=0.0348X + 0.1677$	0.5028***	1.1823	12.34	$y=0.0091X + 0.2543$	0.407***	0.3741	15.58	$y=0.0057X + 0.0003$	0.2966**	0.3027	18.66
	CSM_PH	$Y=3.387e^{0.608X}$	0.571***	1.15714	12.08	$y=0.9582e^{0.6326x}$	0.5899***	0.3268	13.61				
	ExG	$Y= -0.0044X + 7.5553$	0.0051*	1.64685	22.44	$Y=-0.0026X + 2.424$	0.0215*	0.4626	21.99	$Y=0.0012X + 2.2496$	0.0035*	0.7095	33.73
	CIVE	$Y= -0.064X + 13.681$	0.3318***	1.34845	18.37	$Y=-0.0185X + 3.9729$	0.3466***	0.3779	17.97	$Y=-0.0165X + 3.809$	0.1902***	0.5050	24.01
27-Jul-16	ExGR	$Y=0.0768X - 6.2681$	0.4509***	1.2223	16.65	$Y=0.0209X - 1.5764$	0.4156***	0.3574	16.99	$Y=0.0219X - 1.6889$	0.3168***	0.4639	22.05
	COM	$Y=0.0131X + 4.5145$	0.0203**	1.63273	22.24	$Y=0.0017X + 1.6871$	0.004***	0.4666	22.19	$Y=0.0045X + 1.2529$	0.0208***	0.5554	26.40
	CSM_PH	$Y=2.6677e^{0.4409X}$	0.7164***	1.03518	14.10	$Y=0.7652e^{0.4418X}$	0.7123***	0.2784	13.24				
9-Aug-16	ExG	$Y=-0.016X + 8.8814$	0.2048*	1.57891	21.51	$Y=-0.0045X + 2.5618$	0.2155*	0.4337	20.62				
	CSM_PH	$Y=3.0737e^{0.3518X}$	0.3641*	1.62732	22.17	$Y=0.9682e^{0.3122X}$	0.2819*	0.4772	22.69				
18-Aug-16	CSM_PH	$Y=3.8468e^{0.2637X}$	0.4024***	1.19029	22.98	$Y=1.2066e^{0.2299X}$	0.3624***	0.3191	22.79				
	PH _{ref}	$Y=2.0189e^{0.5057X}$	0.7782***	0.84866	11.56	$Y=0.624e^{0.478X}$	0.6826***	0.2787	11.61	$Y=0.9634X - 0.1355$	0.6806***	0.303	11.65
8-Sep-16	CSM_PH	$Y=3.2375e^{0.337X}$	0.608***	1.20095	16.36	$Y=0.9335e^{0.3417X}$	0.5966***	0.3349	13.95				
20-Sep-16	CSM_PH	$Y=2.5238e^{0.4196X}$	0.7206***	0.9984	13.60	$Y=0.7395e^{0.4129X}$	0.6873***	0.2977	12.40				
	PH _{ref}	$Y=1.8826e^{0.5259X}$	0.8112***	0.76207	10.38	$Y=0.5849e^{0.4956X}$	0.7016***	0.2659	11.07	$Y=1.226X - 0.5663$	0.8516***	0.2401	9.14

Note: * Model significance at 0.05 probability level ($p < 0.05$).

** Model significance at 0.01 probability level ($p < 0.01$).

*** Model significance at 0.001 probability level ($p < 0.001$).

Orange colored cells indicate not significant.

Reasonable relationships between the vegetation Indices and biomass/height were measured and different regression equations of biomass and height were established (Table 5). During the early stages (germination and leaf development) and during reproductive and maturity growth stages starting from Stage 7, tasselling (18-Aug-2016) of Figure 4, the Vegetation indices did not have significant relationship with the measured yield at 95% confidence level, therefore the vegetation indices calculated during this periods were not suitable for biomass estimation. The reason is that the vegetation indices which were calculated at the early stages of vegetation growth (that is before 16-June), the background were not covered by vegetation and there were some weeds germinated on the field, so they have mixed reflectance properties with the soil/weeds, but after 16-June chemicals were sprayed on the field to kill the weeds. And starting from the early reproductive stage that is the beginning of tasselling (18-August) the crop starts to turn to brownish/yellowish which affects the reflectance of vegetation and was thus unsuitable for biomass estimation from vegetation indices. Juliane Bendig et al., (2015) also described the visible (RGB) spectral band vegetation indices showed better ability to predict biomass in the early growing stages as compared to the late growth stages. The established models were evaluated their estimation accuracy by their R^2 , RMSE and nRMSE values (Table 5).

Similar to our study Li et al., (2016); Guijarro et al., (2011); and Geipel et al., (2014) also used visible (RGB) band vegetation indices in their studies for crop biomass and plant height estimation. Biomass at harvest time was estimated using different regression models with various vegetation indices derived from visible spectral bands and low correlation was observed between them. This correlation can be improved using multispectral vegetation indices such as NDVI, which have high biomass predicting power. For example, Kross et al., (2015) and Prabhakara et al., (2015) use NDVI vegetation index for biomass estimation with $R^2 > 0.90$.

Referring to the result which was discussed above in Figure 16 and Table 5, for the estimation of biomass, the vegetation indices have generally low correlation with R^2 of ranging from 0.2 to 0.45 this is due to the vegetation indices are highly dependent on the photosynthetically active component of the crops (leaves), but majority of the biomass of maize comes from the stalk and ear which are photosynthetically inactive component. Similar results were also found by Link et al., (2013), in their study they found $R^2 = 0.34$ between vegetation indices and end biomass. This shows that the relationship between biomass and spectral vegetation indices is generally low. But for close growing crops such as barley, the visible band vegetation indices have higher potential in estimating crop height and biomass with higher R^2 ranging from 0.80-0.82 (Juliane Bendig et al., 2015). Similarly, in the study of Li et al., (2016) Visible band vegetation indices show low R^2 for example, CIVE showed a negative relationship in estimating biomass and crop height with $R^2 = 0.35$ for biomass, and $R^2 = 0.15$ for plant height which is comparable to our result, that is $R^2 = 0.34$ for biomass and $R^2 = 0.19$ for plant height.

Based on the result of this study and previous studies the hypothesis 3; the null hypothesis (H_0) was accepted for ExG, CIVE, ExGR, and COM vegetation indices at $\alpha = 0.05$ and for growing stages starting from stage 3 (stem elongation) to stage 6 (flowering, anthesis). But during the early growing stage that is, (before stem elongation, 08-July) and late growing stages (after flowering stage, 09-August), there were no significant relations between VIs and biomass/height, so the alternate hypothesis (H_1) was accepted.

4.3.2. Field Measured Plant Height and Biomass Relationship

Field Measured fresh biomass and oven-dried biomass was plotted against field measured plant height on a scatter plot with an exponential relation. As shown in Figure 17 and table 6 the relationship of the field measured plant height and biomass gives a high correlation of $R^2 = 0.81$ for fresh biomass and $R^2 = 0.70$ for dry biomass. A higher correlation was observed on fresh biomass as compared to dry biomass, this is due to only 20 plants from 20 different plots were used for dry biomass analysis and interpolated for 40 plots and as a result, some errors could occur in calculating dry biomass of all plots.

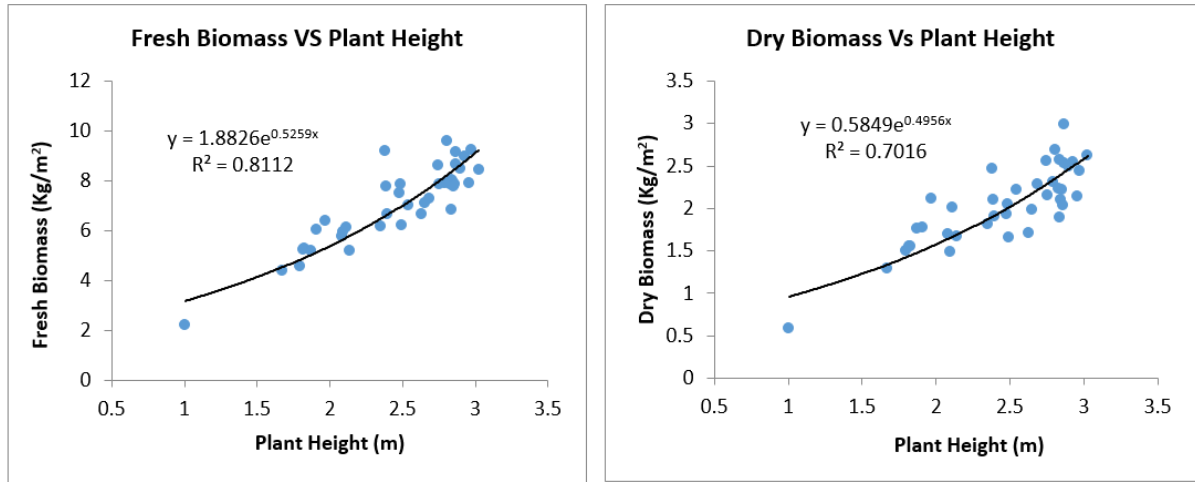


Figure 17: Graphs showing the relationship between field-measured plant height and biomass at physiological maturity (right before harvesting) on sept. 15-23, 2016.

As shown in Table 6 and Figure 17 exponential regression models were derived for fresh and dry biomass versus PH_{CSM} and PH_{ref} and evaluated by their coefficient of determination R^2 . The result showed that a reasonable relationship between PH_{CSM} and Biomass was obtained ($R^2 = 0.72$ for Fresh biomass and $R^2 = 0.68$ for dry biomass). Comparatively, higher correlation was observed with Field measured plant height, PH_{ref} , ($R^2 = 0.81$ for Fresh biomass and $R^2 = 0.70$ for dry biomass), this is because some errors might be introduced due to the CSMs (section 4.2).

Table 6: Coefficient of determination (R^2) for crop heights (PH_{CSM} and PH_{ref} , linear regression) and Plant Height with Fresh and dry biomass (exponential regression) for all plots; at $p < 0.001$. (PH_{CSM} = Crop Surface Model Plant Height; and PH_{ref} = Field measured Plant Height).

	$PH_{CSM}(m)$	$PH_{ref}(m)$	Fresh Biomass (kg/m ²)	Dry Biomass (Kg/m ²)
$PH_{CSM}(m)$	1			
$PH_{ref}(m)$	0.84	1		
Fresh Biomass (kg/m ²)	0.72	0.81	1	
Dry Biomass (Kg/m ²)	0.68	0.70	0.86	1

The descriptive statistics of the field measured plant height and plant height derived from CSMs along with fresh and dry biomass were also described in Table 7. The difference between the mean plant heights derived from Crop Surface Models (PH_{CSMs}) and manually measured plant heights (PH_{ref}) is about 0.17 m and Standard deviation of 0.63 m for PH_{CSM} and 0.46 m for PH_{ref} . The average value of the measured biomass are in the range from 2.24 to 9.58 kg/m² (for fresh biomass) and 0.59 to 2.99 kg/m² (for dry biomass) and shows similar variability with a coefficient variance of 22.25% (fresh) and 22.22% (dry). Based on the field

measurements of 40 maize plots (Table 7), the maize fresh/dry biomass showed a larger spatial variability than field measured plant height with a higher CV ($22.2\% > 18.8\%$) this is due to those plants with the same height could have different biomass. The number of plots for CSMs plant height are shown 27 due to some of the plots lie outside the area coverage of the image captured by the UAVs, and the plant height derived from CSM had higher spatial variability than those of manually measured plant height CV ($27.7\% > 18.8\%$) these variations were aroused from the uncertainty of the generated CSMs.

Table 7: Descriptive statistics field measured plant height and CSMs plant height and aboveground fresh and dry biomass of maize of plots (N=40 for PH_{ref} and biomass; and N=27 for PH_{CSMs}) collected between 15-Sept to 23-Sept-2016, (CV = Coefficient of Variation; SD = Standard Deviation).

	PH _{CSMs} (m)	PH _{ref} (m)	Fresh Biomass (kg/m ²)	Dry Biomass (Kg/m ²)
N	27	40	40	40
Min	0.67	1.004	2.24	0.586828
Max	3.30	3.024	9.58	2.987614
Mean	2.292273	2.460125	7.078875	2.042200643
SD	0.6352586	0.4637864	1.5749625	0.453714059
CV	0.27713045	0.18852149	0.22248768	0.2221691883

4.3.3. Plant Height (PH_{CSM}) modelling for biomass estimation

In addition to the investigation of the relationship between vegetation indices and biomass, the relationship between biomass and crop height were also analyzed and better correlation was observed when plant height was used to estimate biomass. Crop heights at different growth stages were an interesting parameter to describe the crop growth development and to estimate yield/biomass. In this study, the crop heights at different growing stages of the crops were obtained by difference method (which was described in chapter three) of the ground model and the Crop Surface Models (CSMs). Exponential regression models between fresh and dry biomass and plant height derived from CSMs (PH_{CSM}) were developed at different dates and evaluated by their coefficient of determination (R^2), RMSE and nRMSE (Table 5 and Figure 18).

As shown in Table 5 and Figure 18 the relationship of crop height and fresh/dry biomass had higher performance at physiological maturity (ripening stage) with $R^2 = 0.72$ and 0.69 , RMSE of 1.0 kg/m^2 and 0.3 kg/m^2 , and nRMSE of 13.6% and 12.40% for fresh and dry biomass respectively at $p < 0.001$ (Fig. 18f). A better fit was also observed during stem elongation stage, 08-July, ($R^2 = 0.6$) for both fresh and dry biomass (Fig. 18a), similarly, during Inflorescence emergence/heading stage, 27-July, ($R^2 = 0.7$) for both fresh and dry biomass (Fig. 18b). Reasonable relationship was also found during silking/fruit development stage, 08 September, ($R^2 \approx 0.6$) for both fresh and dry biomass (Fig. 18e). But the models for estimating biomass during flowering stage (09-Aug-2016) (Fig. 18c) and tasselling (18-Aug-2016) (Fig. 18d) were weak as compared to others probably due to the low accuracy of the CSM plant height during these periods ($R^2 \approx 0.4$).

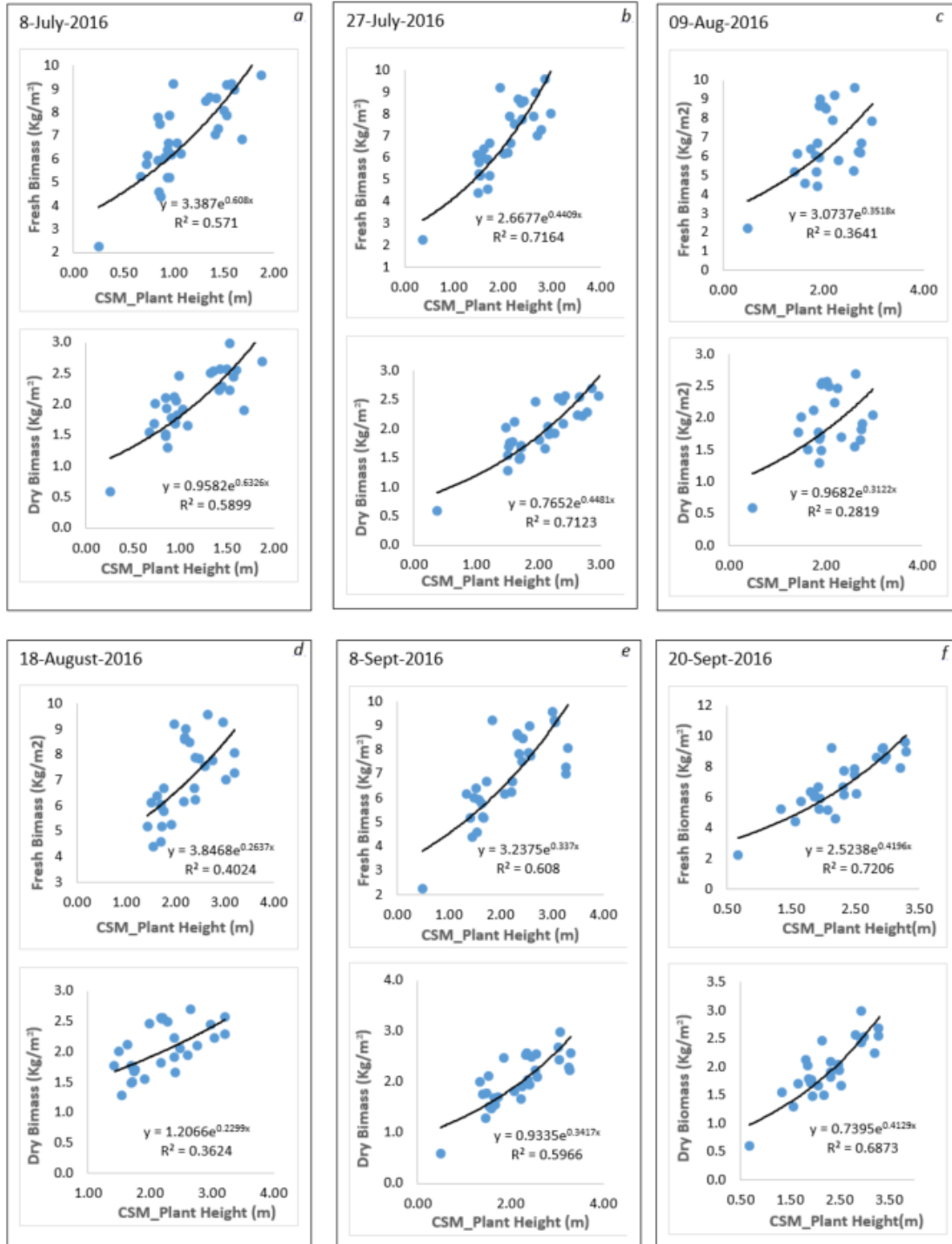


Figure 18: Cross-validation relationships between fresh/dry Biomass and plant height derived from Crop Surface Models (CSMs); $p < 0.001$ for all R² except for 09-Aug-2016, $p < 0.05$.

Based on the results presented in Table 5 and Figure 18 plant height was the most important parameter for fresh and dry biomass estimation of the maize crop. Generally, the predicting ability of the crop height derived from CSMs for fresh and dry biomass increases with vegetation growth development of the crops. The end yield estimation from plant height (PH_{CSM}), during stem elongation stage (08-July) and Inflorescence emergence and heading stage (27-July) (Fig.4), had better performance with higher R² and lower RMSE/nRMSE.

In this study, the PH_{CSM} and manually measured crop height represent the average plant height of all pixels found on each plot. The regression models for biomass estimation from PH_{CSM} performs differently, that is, generally higher R^2 occurs for fresh biomass as compared to dry biomass estimation models. As shown in table 5 the fresh/dry biomass estimation models have lower performance during dates 09-Aug, 18-Aug, and 08-Sept., with R^2 ranging from 0.36 - 0.61 (fresh biomass) and 0.28 - 0.60 (dry biomass), the reason for this was unexpected plant heights were obtained from CSMs during these periods which affects the strength of the relationship. To establish the model the extreme plant heights, that is higher than the expected were removed from the dataset (because these errors were clearly caused due to lack of GCP points on some part of the field). And the height derived from CSMs at the early stages, that is germination and leaf development stages (07-June and 16-June) were not suitable for yield estimation since the heights at this period were too short to use them as biomass estimator.

Similar to our study an Exponential regression equation was used to study the relationship between plant height derived from Crop Surface Models (CSMs) and biomass of barley by Juliane Bendig et al., (2015) and by Yin et al., (2011) for maize biomass estimation. Using UAV-based high-resolution images J. V. Bendig, (2015) also studied the ability of plant height, derived from crop surface models (CSMs), as the best estimator for biomass of barley ($R^2 = 0.81$ for fresh and $R^2 0.82$ for dry). Similarly, Li et al., (2015) studies the estimation of biomass of maize at the peak growth (tasselling stage) using airborne LiDAR-derived canopy height and LAI as input with RMSE = 0.36 kg/m² which was almost similar to the result of this study (RMSE = 0.32 kg/m²) at similar growth stage.

Referring to our result the Crop Surface Models obtained from RGB-based UAV images acquired at different dates have a significant relationship with biomass at the end growing season. So, the plant height data had a general validity to approve its ability for estimating maize biomass non-destructively. Hence the null hypothesis (H_0) of the research hypothesis-4 was accepted.

4.3.4. Biomass modelling from the combined VIs and Plant Height (PH_{CSM})

As mentioned earlier in chapter 3 (section 3.2) a destructive biomass sampling was done at the physiological maturity of the crops just before harvesting to compare with the estimated biomass from VIs and plant height. Stepwise Linear regression models were established between fresh/dry biomass at harvest time as dependent variable and ExG, ExGR and Plant height at different growing stages as an independent variable along with their statistical indicators of R^2 , RMSE and nRMSE values (Table 8). The models were established during the vegetative growth development from early July to mid of August (Fig.4) and are significant at a p-value less than 0.05. As described in section 4.3.1, the vegetation indices calculated before 08-July and after 09-August were not significant at 95% confidence level and not presented in Table 8.

Table 8: Multiple linear regression relationships between fresh/dry biomass as an independent variable and VIs together with CSM plant height as independent variables with their respective R^2 , RMSE, and nRMSE values.

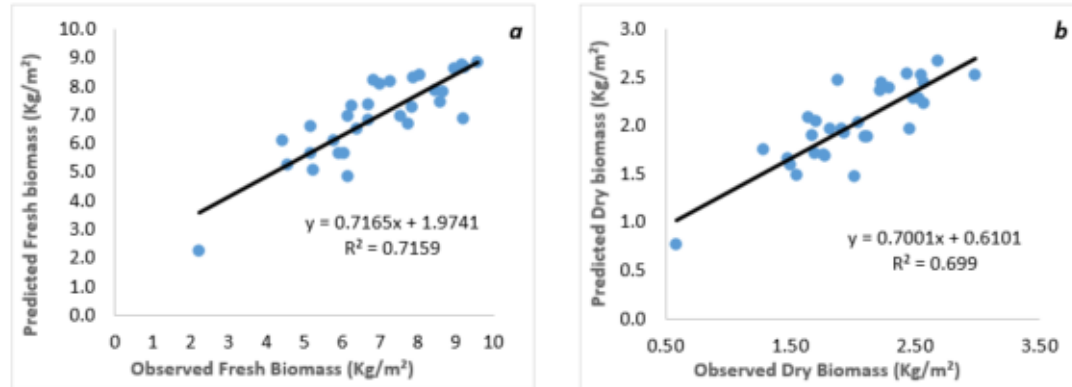
Date	Fresh Biomass/Yield				Dry Biomass/Yield			
	Regression Equation	R^2	RMSE (Kg/m ²)	nRMSE (%)	Regression Equation	R^2	RMSE (Kg/m ²)	nRMSE (%)
8-Jul-16	$Y=0.0201*ExG+2.5581*PH_{CSM}+0.167$	0.7159**	0.8937	12.18	$Y=0.0041*ExG+0.8673*PH_{CSM}+0.2541$	0.699**	0.2665	11.10
27-Jul-16	$Y=0.03394*ExGR+1.9568*PH_{CSM}-2.9633$	0.7537*	0.8186	11.15	$Y=0.0079*ExGR+0.5951*PH_{CSM}-0.5713$	0.7642*	0.2271	10.80
9-Aug-16	$Y=-0.019*ExG+1.939*PH_{CSM}+5.3213$	0.5444**	1.0294	14.02	$Y=-0.0052*ExG+0.4531*PH_{CSM}+1.7298$	0.4581**	0.3105	14.76

Note: * Model significance at 0.05 probability level ($p<0.05$).

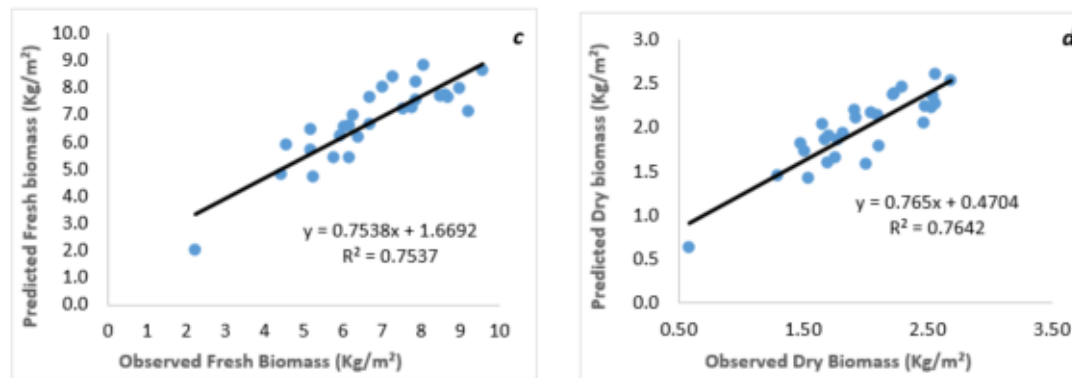
** Model significance at 0.01 probability level ($p<0.01$).

Based on the result of multiple linear regression models shown in Table 8, only ExG vegetation index together with PH_{CSM} was significant at $p < 0.01$ to estimate biomass during the stem elongation (8-July) and flowering stage (9-August), and a regression model was established using these two independent variables. During inflorescence emergence and heading (27-July), only ExGR and PH_{CSM} were found to be significant at $p < 0.05$ for fresh and dry biomass estimation.

08-Jul-2016



27-Jul-2016



09-Aug-2016

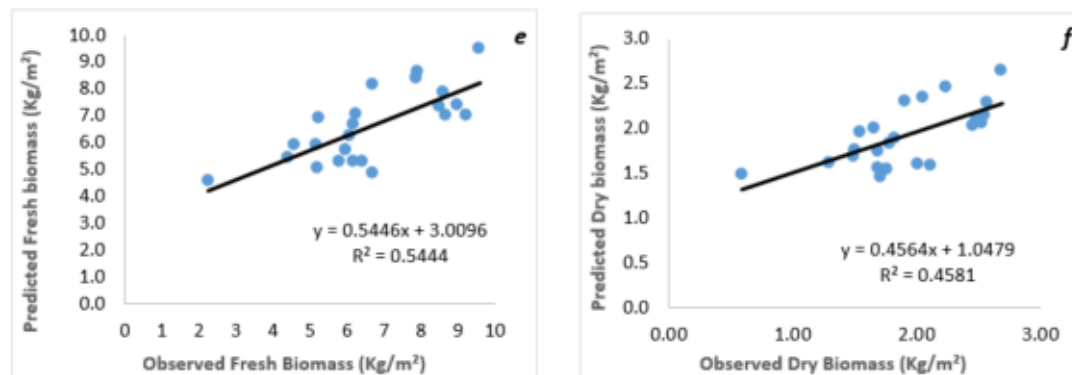


Figure 19: Cross-validation scatter plots for observed fresh and dry biomass versus predicted biomass from the combination of CSM plant height and vegetation indices of dates; 08-Jul-16 (*a&b*); 27-Jul-16 (*c&d*); and 09-Aug-16 (*e&f*).

The general concept of the biomass regression models described in Table 8 was to calculate the fresh and dry biomass and which was validated by comparing the actual and the predicted biomass plotted in Figure 19 by their respective coefficient of determination (R^2). The performance of the regression model (ExGR + PH_{CSM}) at inflorescence emergence, heading stage (27-July) was relatively high with, R^2 of 0.75 and 0.76, and RMSE of 0.82 kg/m² and 0.23 kg/m² for fresh and dry biomass respectively (Fig.19c&d) at $p < 0.05$. During stem elongation (08-July) the model, with ExG and PH_{CSM} variables, had also good performance in predicting biomass with higher R^2 of 0.72 for fresh biomass and 0.70 for dry biomass (Fig. 19a&b) at $p < 0.01$. The predicting ability lowered after growth stage 6, flowering stage (09-Aug) with a little bit lower R^2 and higher RMSE and nRMSE as compared to the previous stages with, $R^2 = 0.54$ and nRMSE = 14.02% for fresh biomass; $R^2 = 0.46$ and nRMSE = 14.76% for dry biomass (Fig.19e&f) at $p < 0.01$.

The multiple regression analysis were carried out to investigate the dependence of the fresh and dry biomass from the combination of plant height and vegetation indices. In general, a moderate correlation was obtained for each individual variable to fresh/dry biomass, but the correlation increases when combined variables (PH_{CSM} and VIs together) were used to estimate yield, that means higher R^2 and lower RMSE were obtained from multiple linear regression models. The combination of plant height derived from Crop Surface Models and vegetation indices allows advanced estimation for fresh and dry biomass (Geipel et al., 2014). The R^2 , RMSE and nRMSE values were used to evaluate the strength of the models in estimating the biomass. And in addition to this, the actual biomass and predicted biomass (fresh/dry) were plotted on a scatter plot to evaluate the predicting ability of the regression models.

Generally, good performance was found for multiple linear regression model combinations PH_{CSM} + ExG (on 08-July), PH_{CSM} + ExGR (on 27-July) and PH_{CSM} + ExG (on 09-August). All correlation had better fit with R^2 above (0.54 and 0.46) and nRMSE below (14.02% and 14.75%) for (fresh and dry) biomass estimation respectively. So multiple linear regression models with combinations of plant heights and vegetation indices give better yield estimation with higher R^2 and lower RMSE and nRMSE values. Comparably, Juliane Bendig et al., (2015) also described in their study that the combined plant height derived from Crop Surface models (PH_{CSM}) and selected vegetation indices fitted in multiple linear regression models performed better than vegetation indices alone with R^2 ranging from 0.78 to 0.82.

4.4. Maize Yield at Harvest

The final pixel based maize biomass was calculated using the equation with combined ExG vegetation index and crop height (derived from CSM) at stem elongation growth stage (08-Jul-16). As shown in table 8 using this regression model the computed RMSE of the actual and predicted biomass was 0.90 kg/m² for fresh biomass and 0.27 kg/m² for dry biomass at $p < 0.01$. The equation that best describe the biomass estimation of maize using VI and crop height relationship was “ $Y = 0.0201 * ExG + 2.5581 * PH_{CSM} + 0.167$ ” for fresh biomass and “ $Y = 0.0041 * ExG + 0.8673 * PH_{CSM} + 0.2541$ ” for dry biomass. The criteria used to select the optimal model was the model with higher R^2 and lower RMSE which was significant at 0.01 probability level.

As shown in the yield map of Figure 20 there is high spatial variability within the field due to variation in crop height, and highest biomass was represented by green color which corresponds to highest crop height. The red and yellow colors also represent for lower biomass. The reason for such variation in biomass within the field was the low growing areas (low plant height) that could be due to water stresses and other environmental factors during the growth period (section 4.2).

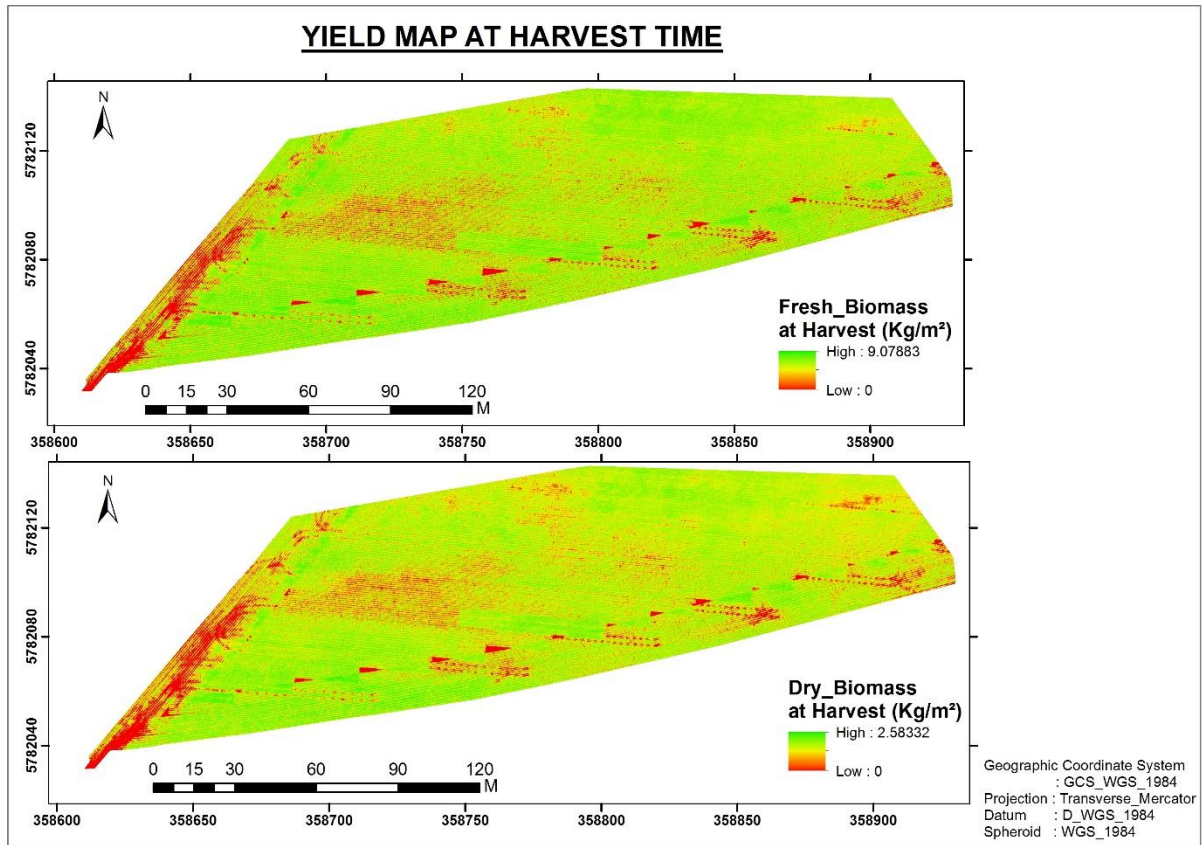


Figure 20: Pixel based yield map resulted from modeling of Excess Green (**ExG**) vegetation index and plant height derived from Crop Surface Model (**PH_{CSM}**) of UAV image acquired during Stem elongation of maize.

The descriptive statistics resulted from the selected model at $\alpha = 0.05$ is described in Table 9, the actual and predicted fresh and dry biomass had almost the same mean approving the models good performance. But the standard deviation of actual and predicted biomass are slightly different with least variation in predicted yield as compared to the variation of actual yield in both Fresh and dry biomass.

Table 9: Descriptive statistics of the actual and predicted biomass (fresh and dry) of maize at harvest (Kg/m^2)

	<i>Fresh Biomass</i>	<i>Predicted Y.</i>	<i>Dry Biomass</i>	<i>Predicted Y.</i>
Mean	6.936	6.944	2.018	2.023
Std. Deviation	1.704	1.443	0.494	0.413
Variance	2.905	2.083	0.244	0.171
Minimum	2.24	2.268	0.587	0.770
Maximum	9.58	8.862	2.988	2.676

95% Confidence Level of the mean

The mean and standard deviation of dry biomass for this study were found to be $2.02 \text{ kg}/\text{m}^2$ and $0.41 \text{ kg}/\text{m}^2$ respectively, with RMSE of $0.27 \text{ kg}/\text{m}^2$. Comparably, Li et al., (2016) estimated above ground biomass of maize with an average of $1.75 \text{ kg}/\text{m}^2$ and standard deviation of $0.86 \text{ kg}/\text{m}^2$.

5. CONCLUSION AND RECOMMENDATION

Based on the results and discussion presented in chapter four of the present study, this section also presents the following parts:

- Conclusions with summary answer to each research question and
- Recommendations for further studies.

5.1. Conclusions

This study demonstrates the potential of very high-resolution multi-temporal UAV images for monitoring crop growth development during the whole growing season for efficient planning and decision making. The primary objective of this thesis is to evaluate UAV-based RGB imaging and its products, like the vegetation indices and plant height derived from crop surface models (PH_{CSM}) for modelling fresh and dry biomass of maize and mapping fractional vegetation cover (FVC) at different growing stages.

Six vegetation indices were tested in mapping Fractional Vegetation Cover (FVC), out of which only two vegetation indices (ExG and COM) were found to be significant in calculating percentage vegetation cover during the first four UVA flights (from germination to inflorescence emergence and heading stage).

Furthermore, these vegetation indices were also evaluated at 95% confidence level for their use to estimate fresh/dry biomass at harvest and crop height at a respective growth stage. Optimal vegetation indices were selected by their strength of correlation with the biomass at harvest time and significant relationship was found with ExG at the stem elongation stage with higher R² and lower RMSE. Next to ExG, the ExGR with the positive relationship and CIVE with negative correlation at inflorescence emergence and heading stage had a reasonable relationship with biomass.

The CSMs was assessed as the predictor for the crop height and biomass at harvest time. It was found that CSMs can accurately estimate crop height with an accuracy between 68% and 85% and can be improved by taking sufficient and well-distributed GCP point on the study site. In addition, crop height derived from UAV-based Crop Surface Models (CSMs) at the different growing stage were evaluated for assessing the biomass at harvest. And the result assured there is a strong correlation between plant height and biomass with higher R² especially during mid of vegetative development. And the predicting ability of crop height is found to be better as compared to vegetation indices.

Answers to the research questions

Q1: *Which vegetation index/indices is/are best for fractional vegetation cover mapping in relation to time/growth stage of the crops?*

- Based on this study, Fractional Vegetation Cover (FVC) can be mapped from germination stage, 07-June (around 0% vegetation cover) to inflorescence emergence and heading stage, 27-July (around 100% vegetation cover) (fig. 4). After July-27, that is from flowering/anthesis stage the ground is totally covered by vegetation. Out of the six vegetation indices tested for mapping FVC, ExG and COM vegetation indices were best in mapping FVC by differentiating the vegetation from its background with higher classification accuracy.

Q2: *What is the accuracy of crop surface models to calculate plant height?*

- To validate the accuracy of plant height estimated from Crop Surface Models (CSMs), this study uses two datasets of different growing stages, that is crop heights measured manually during (13-to-17-Aug) and (15-to-23-Sep) which corresponds with UAV flight of (18-Aug) and (20-Sep) respectively. And found an accuracy of 68% during the first dataset and 85% accuracy during the last campaign. The reason for low accuracy for August 18 is that in some plots the plant heights obtained from CSMs were higher than the expected height. This can be improved by generating accurately georeferenced DSM/CSM by using enough and well-distributed GCP points.

Q3: *Which Vegetation Index is best to estimate maize yield and how is it related to the crop height and yield during the growing season?*

- Based on the results presented in this thesis some of the visible band vegetation indices have a potential in estimating end biomass of maize. As described in chapter 4 the vegetation indices are only significant between 08-July to 09-August (from stem elongation to flowering stage) in estimating biomass and plant height. The ExG vegetation index has better performance at stem elongation stage (08-July) (fig. 4). CIVE and ExGR (at inflorescence emergence and heading stage, 27-July) have also reasonable estimation accuracy next to ExG.

Q4: *What are the relationships of biomass versus crop height derived from CSMs and biomass versus Vegetation indices?*

- A linear regression model with vegetation indices, an exponential relationship with plant height (PH_{CSM}) and stepwise linear regression model using both parameters, Plant height, and vegetation indices was fitted to estimate fresh and dry biomass. The detailed relationships are shown in tables 5 & 8. Multiple linear regression models with a combined plant height and vegetation indices show better biomass estimation performance than models with vegetation indices alone. And except for three flights (09-Aug, 18-Aug, and 08-Sep), due to inaccurate CSMs, the exponential relationship of plant height performs better for biomass estimation with higher $R^2 > 0.71$. And the plant height obtained on 08-July is short enough to estimate end biomass but still, it is significant for estimation ($R^2 \approx 0.60$).

Q5: *Which growth stage or best time to record the crop using UAVs for accurate yield estimation?*

- For efficient management and monitoring of crops during the growing season, it is important to know the best time or growth stage to survey the crops for optimal yield estimation. This is one of the objectives to be assessed by this study, accordingly based on the products obtained from high-resolution multi-temporal UAV images, like CSM plant height and vegetation indices best yield estimations were observed during stem elongation (08-July) and Inflorescence emergence, heading (27-July) stage of figure 4. During this growing stages, fresh and dry biomass can be estimated from both PH_{CSM} and vegetation indices with an error of only (1.2 kg/m² - 1.6 kg/m² for fresh and 0.35 kg/m² - 0.38 kg/m² for dry). Therefore, the best time to record maize field using UAVs for accurate yield estimation is after one month from germination that is stages 3-5 (fig. 4), July in this case.

5.2. Recommendations

The present study investigated and reached a conclusion on estimating fresh and dry biomass using RGB-based vegetation index (ExG) and CSM derived crop height acquired by the UAVs. But in terms of agricultural crop monitoring during the whole growing season, it has some limitations and needs some improvement for improved crop yield/biomass assessment. To improve the assessment of yield using very high-resolution UAV images the following recommendations are suggested for further studies:

- Accurately georeferenced Digital Surface Model (DSM), CSM in this case, should be generated for accurate plant height measurement. This can be achieved by putting well, sufficiently distributed and visible Ground Control Points (GCPs) over the entire field. Or some improvements should be made on the UAV-based image collection by mounting on-board GPS with high accuracy which enables direct geo-referencing of the images, this omits GCP measurement and speeds up data collection and processing.
- This study focusses on multi-temporal analysis which enables accurate monitoring of plant height and plant growth development, but in further studies, hyperspectral analysis should be included to derive physiological plant parameters like Leaf Area Index (LAI), chlorophyll and nitrogen content of the plants which are very important information for monitoring crop growth and studying crop stresses. This can be done using new technologies like hyperspectral camera systems which can provide the above mentioned hyperspectral and 3D spatial information which is powerful for monitoring agricultural crops and biomass estimation.
- In addition to the RGB sensor, in further studies, it is advisable to use NIR camera for UAV by combining high spectral and spatial resolution which are a promising development in further researches and enable a new and advanced crop monitoring possibilities. Because NIR can provide a clear picture of crop health and moisture variations and also have greater opportunity for visual interpretation and digital analysis.
- This study does not consider factors that could affect the end yield, like soil type, fertilizer/chemical treatments, temperature, and rainfall. In further Studies, those factors should be considered in the analysis for accurate yield/ biomass estimation.
- The small area coverage is the main limitation of studies from UAV imagery, so integration of UAV imagery with satellite imageries like Sentinel_2 & 3 (with low spatial resolution as compared to UAV imagery but freely available) or WorldView_1 & 2 (very high resolution but not freely available) can provide promising result with large spatial coverage.
- Different results of vegetation indices might occur because of the lighting condition (sometimes full of sun and sometimes cloudy) during the flight periods which was not studied in this research. So the vegetation indices of different flights were difficult to compare, and more work should be done to calibrate the biomass estimation from these vegetation indices.

LIST OF REFFERENCES

- Ajaere, N. M. (2012). *Multi-Temporal Analysis of Crop Biomass Using Selected Environmental Variables and Remote Sensing Derived Indices*. University of Nebraska-Lincoln. Retrieved from <http://digitalcommons.unl.edu/geographythesis/12/%5Cnpapers2://publication/uuid/2B01EFCD-605C-41A6-BEBF-653CADBF892D>
- Anthony, D., Elbaum, S., Lorenz, A., & Detweiler, C. (2014). On crop height estimation with UAVs. In *IEEE International Conference on Intelligent Robots and Systems* (pp. 4805–4812). <http://doi.org/10.1109/IROS.2014.6943245>
- Barret, R., Crowther, P., Laurence, R., & Lincolne, R. (2000). Agricultural Crop Identification Using Spot and Landsat Images in Tasmania. *Archives of Photogrammetry and Remote Sensing*, XXXIII, 133–139.
- Bendig, J., Bolten, A., & Bareth, G. (2013). UAV-based Imaging for Multi-Temporal, very high Resolution Crop Surface Models to monitor Crop Growth Variability. *Photogrammetrie - Fernerkundung - Geoinformation*, 6, 551–562. <http://doi.org/10.1127/1432-8364/2013/0200>
- Bendig, J., Bolten, A., Bennertz, S., Broscheit, J., Eichfuss, S., & Bareth, G. (2014). Estimating biomass of barley using crop surface models (CSMs) derived from UAV-based RGB imaging. *Remote Sensing*, 6(11), 10395–10412. <http://doi.org/10.3390/rs61110395>
- Bendig, J. V. (2015). *Unmanned aerial vehicles (UAVs) for multi-temporal crop surface modelling. A new method for plant height and biomass estimation based on RGB-imaging*. Universität zu Köln, Germany. Retrieved from http://kups.ub.uni-koeln.de/6018/1/Bendig_PhD_2014_Ort&Datum_final_noCV.pdf
- Bendig, J., Willkomm, M., Tilly, N., Gnyp, M. L., Bennertz, S., Qiang, C., ... Bareth, G. (2013). Very high resolution crop surface models (CSMs) from UAV-based stereo images for rice growth monitoring In Northeast China. *International Archives of the Photogrammetry, Remote Sensing and Spatial Information Sciences*, XL, 4–6. <http://doi.org/10.5194/isprsarchives-XL-1-W2-45-2013>
- Bendig, J., Yu, K., Aasen, H., Bolten, A., Bennertz, S., Broscheit, J., ... Bareth, G. (2015). Combining UAV-based plant height from crop surface models, visible, and near infrared vegetation indices for biomass monitoring in barley. *International Journal of Applied Earth Observation and Geoinformation*, 39, 79–87. <http://doi.org/10.1016/j.jag.2015.02.012>
- Cai, G., Dias, J., & Seneviratne, L. (2014). A Survey of Small-Scale Unmanned Aerial Vehicles: Recent Advances and Future Development Trends. *Unmanned Systems*, 2(2), 175–199. <http://doi.org/10.1142/S2301385014300017>
- Centre for Earth Systems Engineering Research (CESER). (n.d.). UAVs for ESE Applications - CESER - Newcastle University. Retrieved July 27, 2016, from <http://www.ncl.ac.uk/ceser/research/observation/uav-ese-applications/>
- Cui, Y., Luo, Y., & Wang, L. (2011). Extraction of vegetation fraction based on the dimidiate pixel model and vegetation index transform plan. *Photonics and Imaging for Agricultural Engineering*, 7752, 775202-775202–8. <http://doi.org/10.1117/12.886240>
- Dahms, T., Seissiger, S., Conrad, C., & Borg, E. (2016). MODELLING BIOPHYSICAL PARAMETERS OF MAIZE USING LANDSAT 8 TIME SERIES. *The International Archives of the Photogrammetry, Remote Sensing and Spatial Information Sciences*, XLI-B2, 171–175. <http://doi.org/10.5194/isprsarchives-XLI-B2-171-2016>

- Duncan, J. M. A., Dash, J., & Atkinson, P. M. (2015). The potential of satellite-observed crop phenology to enhance yield gap assessments in smallholder landscapes. *Frontiers in Environmental Science*, 3, 1–16. <http://doi.org/10.3389/fenvs.2015.00056>
- Gao, S., Niu, Z., Huang, N., & Hou, X. (2013). Estimating the Leaf Area Index, height and biomass of maize using HJ-1 and RADARSAT-2. *International Journal of Applied Earth Observation and Geoinformation*, 24(1), 1–8. <http://doi.org/10.1016/j.jag.2013.02.002>
- Geipel, J., Link, J., & Claupein, W. (2014). Combined spectral and spatial modeling of corn yield based on aerial images and crop surface models acquired with an unmanned aircraft system. *Remote Sensing*, 6(11), 10335–10355. <http://doi.org/10.3390/rs61110335>
- Gitelson, A. A., Kaufman, Y. J., Stark, R., & Rundquist, D. (2002). Novel algorithms for remote estimation of vegetation fraction. *Remote Sensing of Environment*, 80(1), 76–87. [http://doi.org/10.1016/S0034-4257\(01\)00289-9](http://doi.org/10.1016/S0034-4257(01)00289-9)
- Grenzdörffer, G. J. (2014). Crop height determination with UAS point clouds. *International Archives of the Photogrammetry, Remote Sensing and Spatial Information Sciences - ISPRS Archives*, 40(1), 135–140. <http://doi.org/10.5194/isprsarchives-XL-1-135-2014>
- Guijarro, M., Pajares, G., Riomoros, I., Herrera, P. J., Burgos-Artizzu, X. P., & Ribeiro, A. (2011). Automatic segmentation of relevant textures in agricultural images. *Computers and Electronics in Agriculture*, 75(1), 75–83. <http://doi.org/10.1016/j.compag.2010.09.013>
- Hague, T., Tillett, N. D., & Wheeler, H. (2006). Automated crop and weed monitoring in widely spaced cereals. *Precision Agriculture*, 7(1), 21–32. <http://doi.org/10.1007/s11119-005-6787-1>
- Hoffmeister, D., Bolten, A., Curdt, C., Waldhoff, G., & Bareth, G. (2010). High resolution Crop Surface Models (CSM) and Crop Volume Models (CVM) on field level by terrestrial laser scanning. *SPIE Proceedings*, 7840, 78400E–78400E–6. <http://doi.org/10.1117/12.872315>
- Hunt, E. R., Cavigelli, M., Daughtry, C. S. T., McMurtrey, J. E., & Walthall, C. L. (2005). Evaluation of digital photography from model aircraft for remote sensing of crop biomass and nitrogen status. *Precision Agriculture*, 6(4), 359–378. <http://doi.org/10.1007/s11119-005-2324-5>
- Inglada, J., Arias, M., Tardy, B., Hagolle, O., Valero, S., Morin, D., ... Koetz, B. (2015). Assessment of an Operational System for Crop Type Map Production Using High Temporal and Spatial Resolution Satellite Optical Imagery. *Remote Sensing*, 7(9), 12356–12379. <http://doi.org/10.3390/rs70912356>
- Jain, M., Mondal, P., DeFries, R. S., Small, C., & Galford, G. L. (2013). Mapping cropping intensity of smallholder farms: A comparison of methods using multiple sensors. *Remote Sensing of Environment*, 134, 210–223. <http://doi.org/10.1016/j.rse.2013.02.029>
- Jannoura, R., Brinkmann, K., Uteau, D., Bruns, C., & Joergensen, R. G. (2015). Monitoring of crop biomass using true colour aerial photographs taken from a remote controlled hexacopter. *Biosystems Engineering*, 129, 341–351. <http://doi.org/10.1016/j.biosystemseng.2014.11.007>
- Jin, X., Yang, G., Xu, X., Yang, H., Feng, H., Li, Z., ... Lan, Y. (2015). Combined multi-temporal optical and radar parameters for estimating LAI and biomass in winter wheat using HJ and RADARSAR-2 data. *Remote Sensing*, 7(10), 13251–13272. <http://doi.org/10.3390/rs71013251>
- Kataoka, T., Kaneko, T., Okamoto, H., & Hata, S. (2003). Crop growth estimation system using machine vision. *Proceedings 2003 IEEE/ASME International Conference on Advanced Intelligent Mechatronics (AIM 2003)*, 2, 1079–1083. <http://doi.org/10.1109/AIM.2003.1225492>

- Kross, A., McNairn, H., Lapen, D., Sunohara, M., & Champagne, C. (2015). Assessment of RapidEye vegetation indices for estimation of leaf area index and biomass in corn and soybean crops. *International Journal of Applied Earth Observation and Geoinformation*, *34*(1), 235–248. <http://doi.org/10.1016/j.jag.2014.08.002>
- Lewis, J. E., Rowland, J., & Nadeau, a. (1998). Estimating maize production in Kenya using NDVI: Some statistical considerations. *International Journal of Remote Sensing*, *19*(13), 2609–2617. <http://doi.org/10.1080/014311698214677>
- Li, W., Niu, Z., Chen, H., Li, D., Wu, M., & Zhao, W. (2016). Remote estimation of canopy height and aboveground biomass of maize using high-resolution stereo images from a low-cost unmanned aerial vehicle system. *Ecological Indicators*, *67*, 637–648. <http://doi.org/10.1016/j.ecolind.2016.03.036>
- Li, W., Niu, Z., Huang, N., Wang, C., Gao, S., & Wu, C. (2015). Airborne LiDAR technique for estimating biomass components of maize: A case study in Zhangye City, Northwest China. *Ecological Indicators*, *57*, 486–496. <http://doi.org/10.1016/j.ecolind.2015.04.016>
- Link, J., Senner, D., & Claupein, W. (2013). Developing and evaluating an aerial sensor platform (ASP) to collect multispectral data for deriving management decisions in precision farming. *Computers and Electronics in Agriculture*, *94*, 20–28. <http://doi.org/10.1016/j.compag.2013.03.003>
- Liu, Y., Mu, X., Wang, H., & Yan, G. (2012). A novel method for extracting green fractional vegetation cover from digital images. *Journal of Vegetation Science*, *23*(3), 406–418. <http://doi.org/10.1111/j.1654-1103.2011.01373.x>
- Meier, U. (2001). Growth stages of mono-and dicotyledonous plants. BBCH-Monograph. *Agriculture*, *12*, 141–147 ST. <http://doi.org/10.5073/bbch0515>
- Mesas-Carrascosa, F. J., Torres-Sánchez, J., Clavero-Rumbao, I., García-Ferrer, A., Peña, J. M., Borra-Serrano, I., & López-Granados, F. (2015). Assessing optimal flight parameters for generating accurate multispectral orthomosaics by uav to support site-specific crop management. *Remote Sensing*, *7*(10), 12793–12814. <http://doi.org/10.3390/rs71012793>
- Natural Resources Canada. (2015). Crop Monitoring & Damage Assessment. Retrieved July 29, 2016, from <http://www.nrcan.gc.ca/earth-sciences/geomatics/satellite-imagery-air-photos/satellite-imagery-products/educational-resources/14652>
- Nex, F., & Remondino, F. (2014). UAV for 3D mapping applications: A review. *Applied Geomatics*, *6*(1), 1–15. <http://doi.org/10.1007/s12518-013-0120-x>
- North-Rhine-Westphalia. (2016). In Encyclopædia Britannica. Retrieved August 5, 2016, from <https://www.britannica.com/place/North-Rhine-Westphalia>
- OTSU, N. (1979). A Threshold Selection Method from Gray-Level Histograms. *IEEE Transactions on Systems, Man, Cybernetics*, *9*(1), 62–66.
- Paneque-Gálvez, J., McCall, M. K., Napoletano, B. M., Wich, S. A., & Koh, L. P. (2014). Small drones for community-based forest monitoring: An assessment of their feasibility and potential in tropical areas. *Forests*, *5*(6), 1481–1507. <http://doi.org/10.3390/f5061481>
- PIX4D Support Site. (n.d.). Menu Process > Processing Options... > 1. Initial Processing > General – Support. Retrieved January 17, 2017, from <https://support.pix4d.com/hc/en-us/articles/202557759#gsc.tab=0>

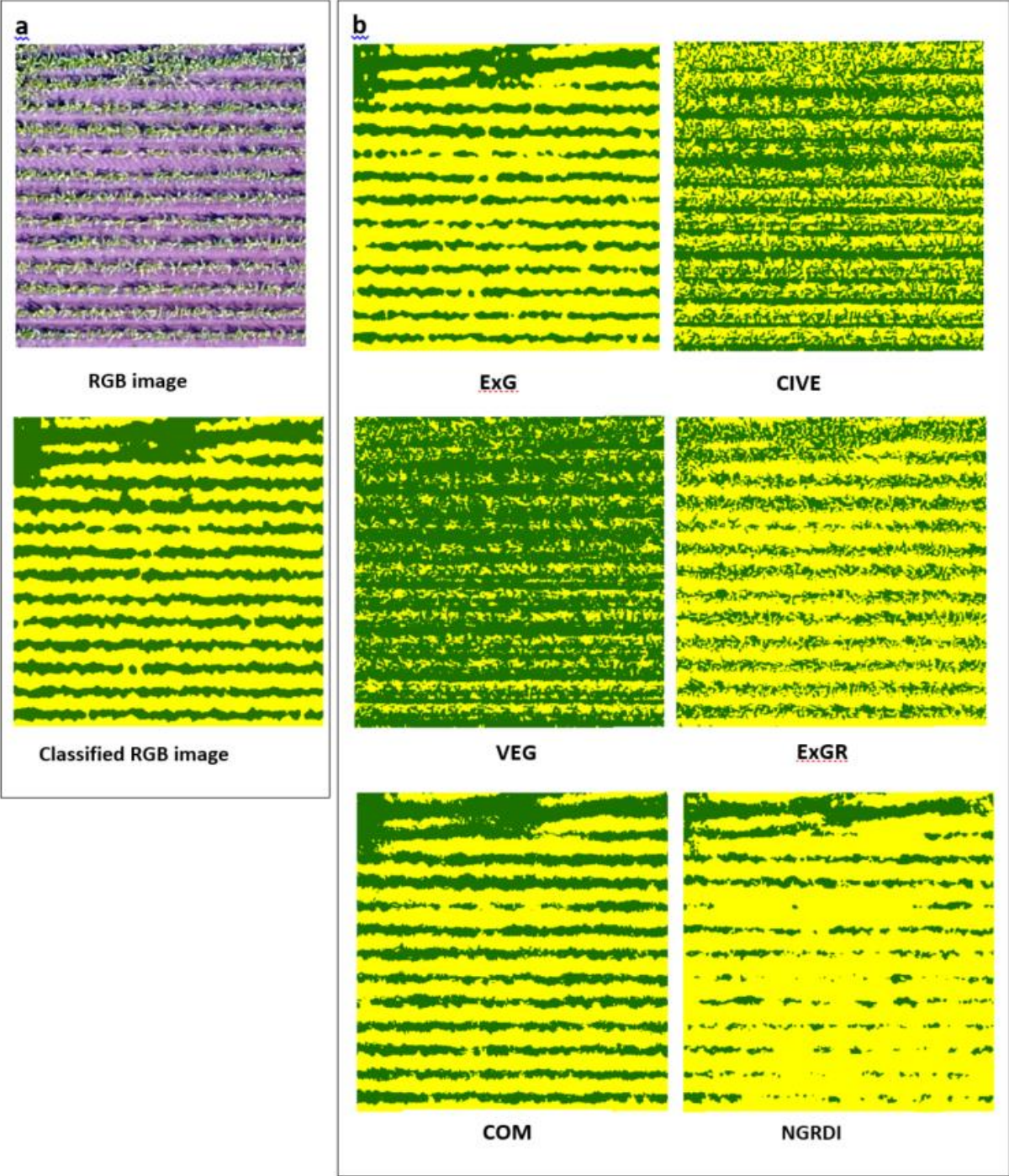
- Prabhakara, K., Dean Hively, W., & McCarty, G. W. (2015). Evaluating the relationship between biomass, percent groundcover and remote sensing indices across six winter cover crop fields in Maryland, United States. *International Journal of Applied Earth Observation and Geoinformation*, 39, 88–102. <http://doi.org/10.1016/j.jag.2015.03.002>
- Ransom, J. (2013). Corn Growth and Management (QUICK GUIDE). *Agronomist – Cereal Crops NDSU Extension Service*, 2, 1–8. Retrieved from <https://www.ag.ndsu.edu/pubs/plantsci/crops/a1173.pdf>
- Reed, B. C., Brown, J. F., VanderZee, D., Loveland, T. R., Merchant, J. W., & Ohlen, D. O. (1994). Measuring Phenological Variability from Satellite Imagery. *Journal of Vegetation Science*, 5, 703–714. <http://doi.org/10.2307/3235884>
- Rembold, F., Atzberger, C., Savin, I., & Rojas, O. (2013). Using low resolution satellite imagery for yield prediction and yield anomaly detection. *Remote Sensing*, 5(4), 1704–1733. <http://doi.org/10.3390/rs5041704>
- Richter, G. M., Agostini, F., Barker, A., Costomiris, D., & Qi, A. (2016). Assessing on-farm productivity of Miscanthus crops by combining soil mapping, yield modelling and remote sensing. *Biomass and Bioenergy*, 85, 252–261. <http://doi.org/10.1016/j.biombioe.2015.12.024>
- Ruiz, J. J., Diaz-Mas, L., Perez, F., & Viguria, A. (2013). Evaluating the Accuracy of Dem Generation Algorithms From Uav Imagery. *International Archives of Photogrammetry and Remote Sensing*, XL-1, 4–6.
- Sharma, L. K., Bu, H., Franzen, D. W., & Denton, A. (2016). Use of corn height measured with an acoustic sensor improves yield estimation with ground based active optical sensors. *Computers and Electronics in Agriculture*, 124, 254–262. <http://doi.org/10.1016/j.compag.2016.04.016>
- Steven, M. D., & Clark, J. A. (2013). *Applications of Remote Sensing in Agriculture*. Kent: Elsevier Science.
- Tellidis, I., & Levin, E. (2014). Photogrammetric Image Acquisition with Small Unmanned Aerial Systems. In *Asprs.Org*. Retrieved from <http://www.asprs.org/a/publications/proceedings/Louisville2014/tellidis.pdf>
- Tilly, N. (2015). *Terrestrial laser scanning for crop monitoring - Capturing 3D data of plant height for estimating biomass at field scale*. Universität zu Köln, Germany.
- Tilly, N., Hoffmeister, D., Cao, Q., Lenz-Wiedemann, V., Miao, Y., & Bareth, G. (2013). Precise plant height monitoring and biomass estimation with Terrestrial Laser Scanning in paddy rice. *ISPRS Annals of Photogrammetry, Remote Sensing and Spatial Information Sciences*, II-5/W2, 295–300. <http://doi.org/10.5194/isprsannals-II-5-W2-295-2013>
- Torres-Sánchez, J., López-Granados, F., De Castro, A. I., & Peña-Barragán, J. M. (2013). Configuration and Specifications of an Unmanned Aerial Vehicle (UAV) for Early Site Specific Weed Management. *PLoS ONE*, 8(3). <http://doi.org/10.1371/journal.pone.0058210>
- Torres-Sánchez, J., Peña, J. M., de Castro, A. I., & López-Granados, F. (2014). Multi-temporal mapping of the vegetation fraction in early-season wheat fields using images from UAV. *Computers and Electronics in Agriculture*, 103, 104–113. <http://doi.org/10.1016/j.compag.2014.02.009>
- Vaudour, E., Noirot-Cosson, P. E., & Membrive, O. (2015). Early-season mapping of crops and cultural operations using very high spatial resolution Pléiades images. *International Journal of Applied Earth Observation and Geoinformation*, 42, 128–141. <http://doi.org/10.1016/j.jag.2015.06.003>
- Vergara-díaz, O., Zaman-allah, M. A., Masuka, B., Hornero, A., Zarco-Tejada, P., Prasanna, B. M., ... Araus, J. L. (2016). A Novel Remote Sensing Approach for Prediction of Maize Yield Under Different Conditions of Nitrogen Fertilization. *Frontiers in Plant Science*, 7, 1–13. <http://doi.org/10.3389/fpls.2016.00666>

- Waypoint Drone Insight and Inspiration. (2015). Using a Drone's Surface Model to Estimate Crop Yields & Assess Plant Health. Retrieved August 20, 2016, from <http://waypoint.sensefly.com/drone-surface-model-estimate-crop-yield-plant-health/>
- Yang, C., Everitt, J. H., & Murden, D. (2010). Evaluating high resolution SPOT 5 satellite imagery for crop identification (Vol. 75). <http://doi.org/http://dx.doi.org/10.1016/j.compag.2010.12.012>
- Yin, X., McClure, M. A., Jaja, N., Tyler, D. D., & Hayes, R. M. (2011). In-season prediction of corn yield using plant height under major production systems. *Agronomy Journal*, *103*(3), 923–929. <http://doi.org/10.2134/agronj2010.0450>
- Yu, Z., Cao, Z., Wu, X., Bai, X., Qin, Y., Zhuo, W., ... Xue, H. (2013). Automatic image-based detection technology for two critical growth stages of maize: Emergence and three-leaf stage. *Agricultural and Forest Meteorology*, *174–175*, 65–84. <http://doi.org/10.1016/j.agrformet.2013.02.011>
- Zaman-Allah, M., Vergara, O., Araus, J. L., Tarekegne, A., Magorokosho, C., Zarco-Tejada, P. J., ... Cairns, J. (2015). Unmanned aerial platform-based multi-spectral imaging for field phenotyping of maize. *Plant Methods*, *11*(1), 35. <http://doi.org/10.1186/s13007-015-0078-2>
- Zhang, C., & Kovacs, J. M. (2012). The application of small unmanned aerial systems for precision agriculture: A review. *Precision Agriculture*, *13*(6), 693–712. <http://doi.org/10.1007/s11119-012-9274-5>

APPENDICES

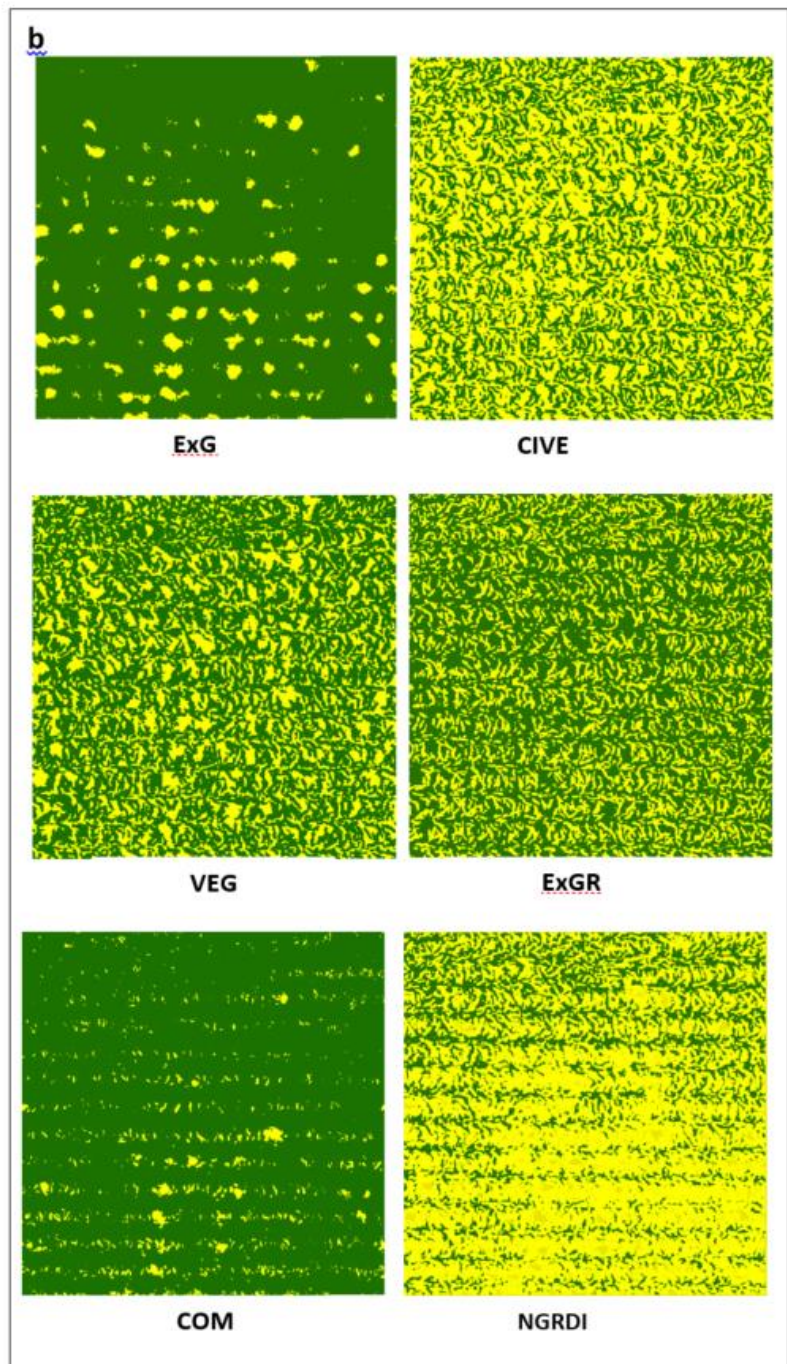
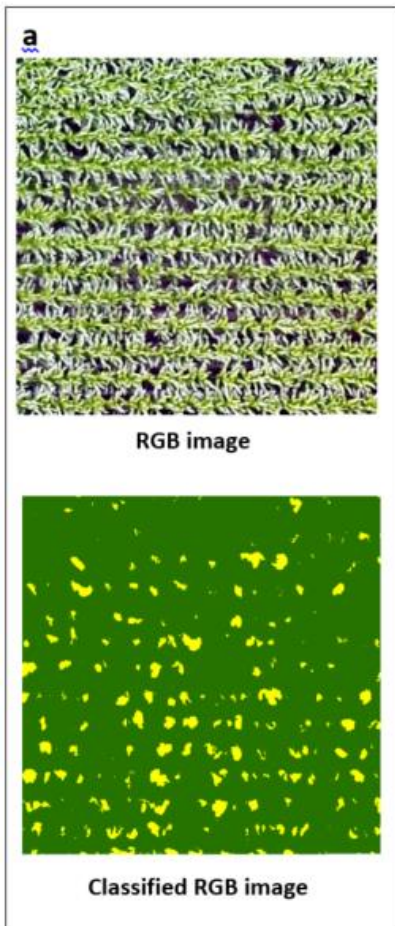
Appendix- 1A

June 16, 2016



Appendix- 1B

July 08, 2016



Appendix - 2

Quality Report


Generated with Pro version 2.2.25

! **Important:** Click on the different icons for:

- ?** Help to analyze the results in the Quality Report
- i** Additional information about the sections

💡 Click [here](#) for additional tips to analyze the Quality Report

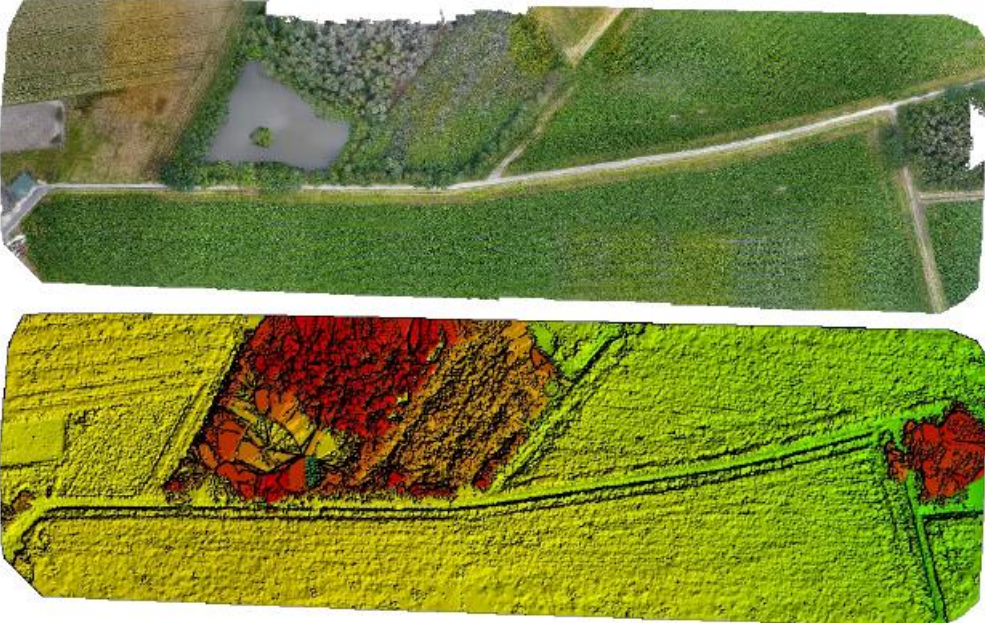
Summary **i**

Project	flight_4
Processed	2016-11-01 23:19:20
Camera Model Name(s)	FC330_3.6_4000x3000 (RGB)
Average Ground Sampling Distance (GSD)	2.12 cm / 0.83 in
Area Covered	0.143 km ² / 14.2974 ha / 0.0552 sq. mi. / 35.3479 acres

Quality Check **i**

? Images	median of 9958 keypoints per image	⚠️
? Dataset	505 out of 515 images calibrated (98%), all images enabled	✅
? Camera Optimization	0.41% relative difference between initial and optimized internal camera parameters	✅
? Matching	median of 3513.83 matches per calibrated image	✅
? Georeferencing	yes, 3 GCPs (3 3D), mean RMS error = 0 m	✅

? Preview **i**



The figure displays two side-by-side aerial views of a rural landscape. The top image is an orthomosaic showing a mix of green fields, a grey pond, and a dirt road. The bottom image is a sparse Digital Surface Model (DSM) of the same area, where terrain elevation is represented by a color gradient from green (low) to red (high), with black lines indicating the sparse point cloud data.

Figure 1: Orthomosaic and the corresponding sparse Digital Surface Model (DSM) before densification.

Calibration Details

Number of Calibrated Images	505 out of 515
Number of Geolocated Images	515 out of 515

Initial Image Positions

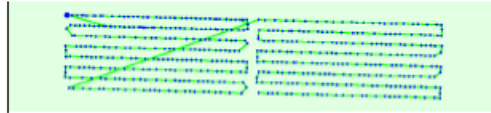
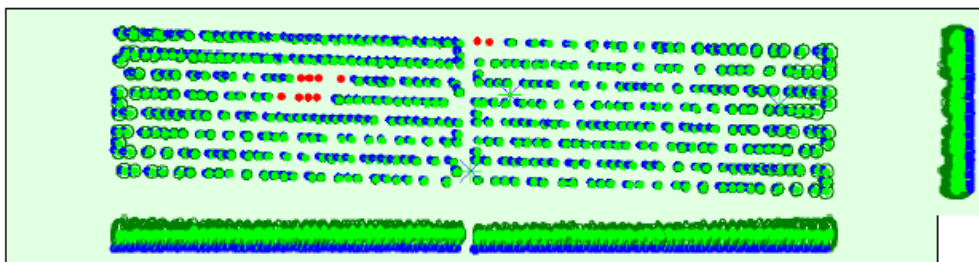


Figure 2: Top view of the initial image position. The green line follows the position of the images in time starting from the large blue dot.

Computed Image/GCPs/Manual Tie Points Positions



Uncertainty ellipses 5x magnified

Figure 3: Offset between initial (blue dots) and computed (green dots) image positions as well as the offset between the GCPs initial positions (blue crosses) and their computed positions (green crosses) in the top-view (XY plane), front-view (XZ plane), and side-view (YZ plane). Red dots indicate disabled or uncalibrated images. Dark green ellipses indicate the absolute position uncertainty of the bundle block adjustment result.

Absolute camera position and orientation uncertainties

	X [m]	Y [m]	Z [m]	Omega [degree]	Phi [degree]	Kappa [degree]
Mean	0.822	0.811	1.823	1.426	0.553	0.294
Sigma	0.190	0.190	0.387	0.006	0.158	0.096

Overlap

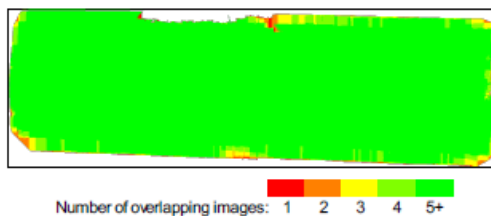


Figure 4: Number of overlapping images computed for each pixel of the orthomosaic. Red and yellow areas indicate low overlap for which poor results may be generated. Green areas indicate an overlap of over 5 images for every pixel. Good quality results will be generated as long as the number of keypoint matches is also sufficient for these areas (see Figure 5 for keypoint matches).

Bundle Block Adjustment Details



Number of 2D Keypoint Observations for Bundle Block Adjustment	1662952
Number of 3D Points for Bundle Block Adjustment	567233
Mean Reprojection Error [pixels]	0.148

Internal Camera Parameters

FC330_3.6_4000x3000 (RGB). Sensor Dimensions: 6.317 [mm] x 4.738 [mm]



EXIF ID: FC330_3.6_4000x3000

	Focal Length	Principal Point x	Principal Point y	R1	R2	R3	T1	T2
Initial Values	2356.592 [pixel] 3.722 [mm]	2000.000 [pixel] 3.159 [mm]	1499.997 [pixel] 2.369 [mm]	-0.001	-0.002	0.000	-0.001	-0.001
Optimized Values	2366.331 [pixel] 3.737 [mm]	2008.698 [pixel] 3.172 [mm]	1274.573 [pixel] 2.013 [mm]	-0.005	0.002	-0.001	-0.000	0.000
Uncertainties (Sigma)	1.047 [pixel] 0.002 [mm]	7.127 [pixel] 0.011 [mm]	7.587 [pixel] 0.012 [mm]	0.001	0.001	0.001	0.001	0.001



The number of Automatic Tie Points (ATPs) per pixel averaged over all images of the camera model is color coded between black and white. White indicates that, in average, more than 16 ATPs are extracted at this pixel location. Black indicates that, in average, 0 ATP has been extracted at this pixel location. Click on the image to see the average direction and magnitude of the reprojection error for each pixel. Note that the vectors are scaled for better visualization.

2D Keypoints Table



	Number of 2D Keypoints per Image	Number of Matched 2D Keypoints per Image
Median	9958	3514
Mn	5981	149
Max	13419	6633
Mean	9938	3293

3D Points from 2D Keypoint Matches



	Number of 3D Points Observed
In 2 Images	360985
In 3 Images	105597
In 4 Images	42648
In 5 Images	20666
In 6 Images	11266
In 7 Images	6784
In 8 Images	4412
In 9 Images	3200
In 10 Images	2325
In 11 Images	1801
In 12 Images	1312
In 13 Images	934
In 14 Images	860
In 15 Images	665
In 16 Images	564
In 17 Images	469
In 18 Images	398
In 19 Images	355
In 20 Images	318

In 21 Images	258
In 22 Images	245
In 23 Images	266
In 24 Images	198
In 25 Images	152
In 26 Images	160
In 27 Images	137
In 28 Images	102
In 29 Images	76
In 30 Images	46
In 31 Images	20
In 32 Images	6
In 33 Images	3
In 34 Images	2
In 35 Images	3

2D Keypoint Matches

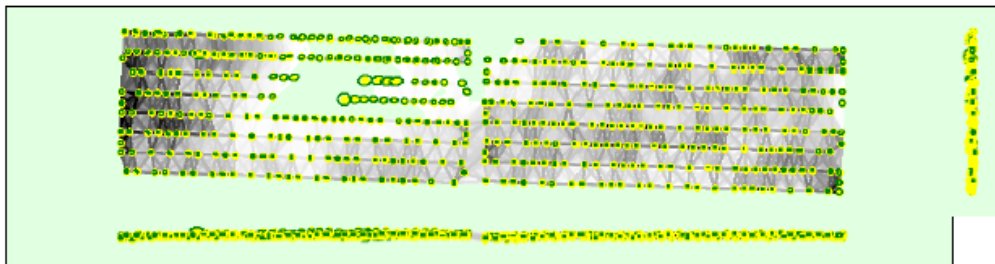


Figure 5: Computed image positions with links between matched images. The darkness of the links indicates the number of matched 2D keypoints between the images. Bright links indicate weak links and require manual tie points or more images. Dark green ellipses indicate the relative camera position uncertainty of the bundle block adjustment result.

Relative camera position and orientation uncertainties

	X[m]	Y[m]	Z[m]	Omega [degree]	Phi [degree]	Kappa [degree]
Mean	0.156	0.137	0.104	0.120	0.131	0.077
Sigma	0.075	0.054	0.050	0.049	0.078	0.036

Geolocation Details

Ground Control Points

GCP Name	Accuracy XY/Z [m]	Error X [m]	Error Y [m]	Error Z [m]	Projection Error [pixel]	Verified/Marked
GPS0006 (3D)	0.020/ 0.020	0.000	0.000	-0.000	0.238	29 / 29
GPS0004 (3D)	0.020/ 0.020	0.000	0.001	-0.000	0.816	6 / 6
GPS0002 (3D)	0.020/ 0.020	-0.000	-0.001	0.000	0.324	33 / 33
Mean [m]		0.000003	0.000047	-0.000014		
Sigma [m]		0.000338	0.001102	0.000064		
RMS Error [m]		0.000339	0.001103	0.000065		

1 out of 4 check points have been labeled as inaccurate.

Check Point Name	Accuracy XY/Z [m]	Error X [m]	Error Y [m]	Error Z [m]	Projection Error [pixel]	Verified/Marked
------------------	-------------------	-------------	-------------	-------------	--------------------------	-----------------

GPS0007	0.0200/0.0200	-0.0164	0.2322	-0.1981	0.2473	21 / 21
GPS0005	0.0200/0.0200	-0.0037	-0.2145	0.2464	0.5831	12 / 12
GPS0003	0.0200/0.0200	-0.0469	-0.0054	0.0209	0.3798	24 / 24
Mean [m]		-0.022326	0.004103	0.023034		
Sigma [m]		0.018107	0.182507	0.181465		
RMS Error [m]		0.028745	0.182553	0.182921		

Localisation accuracy per GCP and mean errors in the three coordinate directions. The last column counts the number of calibrated images where the GCP has been automatically verified vs. manually marked.

? Absolute Geolocation Variance



Min Error [m]	Max Error [m]	Geolocation Error X[%]	Geolocation Error Y[%]	Geolocation Error Z[%]
-	-15.00	0.00	0.00	0.00
-15.00	-12.00	0.00	0.00	0.00
-12.00	-9.00	0.00	0.00	0.00
-9.00	-6.00	0.00	0.00	0.00
-6.00	-3.00	2.18	0.00	0.20
-3.00	0.00	47.13	57.62	47.72
0.00	3.00	50.10	41.98	51.68
3.00	6.00	0.59	0.40	0.40
6.00	9.00	0.00	0.00	0.00
9.00	12.00	0.00	0.00	0.00
12.00	15.00	0.00	0.00	0.00
15.00	-	0.00	0.00	0.00
Mean [m]		-3.626820	1.487506	-12.418860
Sigma [m]		1.425468	0.574693	1.138618
RMS Error [m]		3.896894	1.594662	12.470948

Min Error and Max Error represent geolocation error intervals between -1.5 and 1.5 times the maximum accuracy of all the images. Columns X, Y, Z show the percentage of images with geolocation errors within the predefined error intervals. The geolocation error is the difference between the initial and computed image positions. Note that the image geolocation errors do not correspond to the accuracy of the observed 3D points.

Geolocation Bias	X	Y	Z
Translation [m]	-3.626820	1.487506	-12.418860

Bias between image initial and computed geolocation given in output coordinate system.

? Relative Geolocation Variance



Relative Geolocation Error	Images X[%]	Images Y[%]	Images Z[%]
[-1.00, 1.00]	100.00	100.00	100.00
[-2.00, 2.00]	100.00	100.00	100.00
[-3.00, 3.00]	100.00	100.00	100.00
Mean of Geolocation Accuracy [m]	5.000000	5.000000	10.000000
Sigma of Geolocation Accuracy [m]	0.000000	0.000000	0.000000

Images X, Y, Z represent the percentage of images with a relative geolocation error in X, Y, Z.

Geolocation Orientational Variance	RMS [degree]
Omega	0.544
Phi	2.595
Kappa	1.114

Geolocation RMS error of the orientation angles given by the difference between the initial and computed image orientation angles.

Initial Processing Details



System Information



Hardware	CPU: Intel(R) Xeon(R) CPU E3-1270 v3 @ 3.50GHz RAM: 32GB GPU: RDPUDD Chained DD (Driver: unknown)
Operating System	Windows Server 2012 R2 Datacenter, 64-bit

Coordinate Systems



Image Coordinate System	WGS84 (egm96)
Ground Control Point (GCP) Coordinate System	WGS84 / UTMzone 32N (egm96)
Output Coordinate System	WGS84 / UTMzone 32N (egm96)

Processing Options



Detected Template	No Template Available
Keypoints Image Scale	Custom, Image Scale: 0.5
Advanced: Matching Image Pairs	Aerial Grid or Corridor
Advanced: Matching Strategy	Use Geometrically Verified Matching: yes
Advanced: Keypoint Extraction	Targeted Number of Keypoints: Automatic
Advanced: Calibration	Calibration Method: Standard Internal Parameters Optimization: All External Parameters Optimization: All Rematch: Auto, no

Point Cloud Densification details



Processing Options



Image Scale	multiscale, 1/2 (Half image size, Default)
Point Density	Optimal
Minimum Number of Matches	3
3D Textured Mesh Generation	yes
3D Textured Mesh Settings:	Resolution: Medium Resolution (default) Color Balancing: no
Advanced: 3D Textured Mesh Settings	Sample Density Divider: 1 Maximum Number of Triangles per Leaf: 8
Advanced: Matching Window Size	7x7 pixels
Advanced: Image Groups	group1
Advanced: Use Processing Area	yes
Advanced: Use Annotations	yes
Advanced: Limit Camera Depth Automatically	no
Advanced: Point Cloud Classification (Beta)	yes Minimum Object Length [m]: 0.1 Maximum Object Length [m]: 400 Minimum Object Height [m]: 0.1
Time for Point Cloud Densification	04h:10m:26s
Time for Point Cloud Classification	01h:01m:59s
Time for 3D Textured Mesh Generation	38m:15s

Results



Number of Generated Tiles	5
Number of 3D Densified Points	44615972
Average Density (per m ³)	324.99

DSM, Orthomosaic and Index Details



Processing Options



DSM and Orthomosaic Resolution	1 x GSD (2.13 [cm/pxel])
DSM Filters	Noise Filtering: yes Surface Smoothing: yes, Type: Sharp
Raster DSM	Generated: yes Method: Inverse Distance Weighting Merge Tiles: yes
Orthomosaic	Generated: yes Merge Tiles: yes GeoTIFF Without Transparency: no Google Maps Tiles and KML: yes
Grid DSM	Generated: yes, Spacing [cm]: 100
Time for DSM Generation	59m:51s
Time for Orthomosaic Generation	04h:11m:17s